To the Graduate Council:

I am submitting herewith a thesis written by Cynthia Lee Brown entitled "Characterization of Vitronectin and Plasminogen Activator Inhibitor Type 1: Insights into Metal Binding, and Production of Reagents to Facilitate Structural Studies." I have examined the final electronic copy of this thesis for form and content and recommend that it be accepted in partial fulfillment of the requirements for the degree of Master of Science, with a major in Biochemistry and Cellular and Molecular Biology.

Cynthia B. Peterson, Major Professor

We have read this thesis
and recommend its acceptance:

Engin Serpersu

Nitin Jain

Accepted for the Council:

Carolyn R. Hodges,

Vice Provost and Dean of the Graduate School

(Original signatures are on file with official student records.)

Characterization of Vitronectin and Plasminogen Activator Inhibitor Type 1: Insights into Metal Binding, and Production of Reagents to Facilitate Structural Studies

A Thesis Presented for
the Master of Science Degree
The University of Tennessee, Knoxville

Cynthia Lee Brown
December 2008

DEDICATION

This work is dedicated to my dear friend, Chip Sommer, who has helped me in countless ways, all while making me smile. I also dedicate this to my parents, Floyd and Virginia Brown: my constant supporters and encouragers, and a great source of genes.

ACKNOWLEDGEMENTS

I wish to thank my mentor, Cynthia Peterson, for her guidance and support and for giving me the opportunity to work on the projects I found interesting. I thank my other committee members, Engin Serpersu and Nitin Jain, for their advice and contribution to my education. I am gratefully indebted to the support received from the University of Tennessee Center of Excellence in Structural Biology Fellowship.

ABSTRACT

Vitronectin is a multifunctional glycoprotein involved in regulation of such processes as hemostasis, cell migration, immunity, and tumor metastasis. Many of its functions require interaction with various binding partners. One such partner, plasminogen activator inhibitor-type 1 (PAI-1), belongs to the serine protease inhibitor (serpin) superfamily of proteins. PAI-1 helps regulate hemostasis by affecting blood clot breakdown, and helps regulate cell migration and tissue remodeling by affecting extracellular matrix digestion. Our laboratory is pursuing structural information on vitronectin and the complex formed between vitronectin and PAI-1. To this end, the work presented in this thesis focuses on two aims: characterizing the interaction of vitronectin and PAI-1 with metal ions, and developing reagents to be used in structural studies of vitronectin. We have used electron paramagnetic resonance (EPR) spectroscopy to study metal binding by vitronectin and PAI-1. We have tested vitronectin and PAI-1 for binding of Mn^{2+} and Cu^{2+}, and also established the feasibility of studying protein-Cu^{2+} interaction in solution by EPR, using bovine serum albumin (BSA) and Cu^{2+}. In another set of experiments, we have used activity assays to assess the effect of metal ions on PAI-1 activity and on stabilization of PAI-1 by vitronectin. Regarding reagents, we have expressed and purified active, perdeuterated PAI-1, which can be used in complex with vitronectin in neutron scattering and NMR experiments. We characterized several monoclonal antibodies to vitronectin, and identified one suitable for use in co-crystallization screens. These accomplishments will aid in development of a more detailed picture of the interaction between vitronectin and PAI-1.

TABLE OF CONTENTS

CHAPTER 1 1
Introduction to Vitronectin and Plasminogen Activator Inhibitor Type 1; Statement of Research Objectives 1
Introduction 1
Overview of Vitronectin 1
Domain Structure of Vitronectin 2
Overview of PAI-1 8
Development of Thought on Vitronectin: A Story of Convergent Experimental Paths 12
Beginnings of the cell adhesion path of study 12
Beginnings of the complement system path of study 13
Advances in the cell adhesion path of study 14
Convergence of the two paths 17
The early shared path: A rocky road 19
Questions regarding the functions and interactions of vitronectin and PAI-1 20
Research Objectives 20
Specific Aim 1 20
Specific Aim 2 21
CHAPTER 2 22
Characterization of Vitronectin and PAI-1 Metal Binding 22
Introduction 22
Evidence of Metal Binding 22
Electron Paramagnetic Resonance Studies 26
Kinetic Assay for PAI-1 Activity and Stability 28
Materials and Methods 29
Materials 29
Preparation of Protein for EPR Experiments 29
EPR Spectroscopy 31
Kinetic Assay for PAI-1 Activity and Stabilization by Vitronectin 32
Calculation of Standard Error 33
Results 33
Metal binding assessment by EPR 33
Mg^{2+} has no measurable effect on PAI-1 activity or on stabilization by vitronectin 52
Discussion and Future Directions 55
Metal-binding studies 55
Absence of Mg^{2+} effect on PAI-1 activity and on stabilization by vitronectin 61
CHAPTER 3 63
Expression, Purification and Testing of Perdeuterated PAI-1 63
Introduction 63
Materials and Methods 66
Materials 66
Expression and Purification of Recombinant PAI-1 (wild-type and 14-1B mutant) 66
Expression of Deuterated 14-1B PAI-1 68
SDS-PAGE and Western Blotting 68

tPA Activity Assay 69
PAI-1-tPA Binding Assay 69
Dynamic Light Scattering 70
Results and Discussion 70
PAI-1 Expression and Purification 70
PAI-1 Activity Testing 72
Confirmation of protein monodispersity 74
Future Directions 77
CHAPTER 4 78
Characterization of Monoclonal Antibodies to Vitronectin and Crystallization Screen of Vn-mAb Complex 78
Introduction 78
Materials and Methods 79
Materials 79
Non-competitive ELISA Titrations of Anti-vitronectin Monoclonal Antibodies 79
Competitive ELISA Titrations of Anti-vitronectin Monoclonal Antibodies 80
Characterization of Vn-mAb Complexes by HPLC 81
Crystallization Screen of Vn-1E9 Complex 81
SDS-PAGE 82
Results and Discussion 82
Characterization of Antibodies by ELISA 82
Characterization of Vn-mAb Complexes by HPLC 83
Crystallization Screen of Vn-1E9 Complex 86
Concluding Remarks and Future Directions 90
List of References 91
Vita 97

LIST OF TABLES

Table 1: Proteins and metals tested by EPR 34
Table 2: Summary of anti-vitronectin mAb characterization 88

LIST OF FIGURES

Figure 1: Domain structure predictions for vitronectin obtained from sequence-structure alignment and fold recognition (threading). 3
Figure 2: SAXS Model of Vitronectin. 4
Figure 3: Vitronectin domains and locations of key ligand binding sites. 5
Figure 4: NMR Solution structure of the SMB domain of vitronectin. 7
Figure 5: Active and latent forms of PAI-1. 10
Figure 6: Composite elution profile for PAI-1 bound to five metal-affinity columns. 23
Figure 7: Putative metal-binding site on PAI-1. 25
Figure 8: The EPR spectrum of Mn^{2+} has six distinct peaks. 36
Figure 9: EPR spectrum for 200 μM Cu^{2+}. 37
Figure 10: Standard curve for Cu^{2+} EPR peak intensity. 38
Figure 11: Test for Cu^{2+}-binding by BSA. 40
Figure 12: EPR spectrum for 150 μM Cu^{2+} showing the height (h) used as a measure of concentration. 42
Figure 13: Overlaid EPR spectra for 75 to 300 μM Cu^{2+}. 44
Figure 14: EPR spectra for (*A*) 100 μM and (*B*) 150 μM Cu^{2+}, with and without 25 μM PAI-1. 45
Figure 15: EPR spectra for (*A*) 200 μM and (*B*) 300 μM Cu^{2+}, with and without 25 μM PAI-1. 46
Figure 16: Test for Cu^{2+}-binding by 25 μM PAI-1. 47
Figure 17: Scatchard plot for Cu^{2+}-binding by 25 μM PAI-1. 48
Figure 18: Test for Mn^{2+}-binding by 34 μM Vn. 49
Figure 19: Test for Mn^{2+}-binding by 30 μM PAI-1. 50
Figure 20: Test for Mn^{2+}-binding by 20 μM PAI-1-Vn. 51
Figure 21: Kinetic assay to test PAI-1 activity. 53
Figure 22: Kinetic assay to measure activity of PAI-1 +/- Mg^{2+}. 56
Figure 23: Kinetic assay to measure activity of PAI-1-Vn +/- Mg^{2+}. 57
Figure 24: Kinetic assay to measure activity of PAI-1 +/- Vn. 58
Figure 25: Growth curves for *E. coli* in unlabeled media. 71
Figure 26: D-14-1B PAI-1 binding of tPA is comparable to H-14-1B PAI-1 binding of tPA. 73
Figure 27: Activity of D-14-1B PAI-1 is comparable to activity of H-PAI-1. 75
Figure 28: Dynamic light scattering characterization of PAI-1. 76
Figure 29: Anti-Vn mAb titrations by ELISA. 84
Figure 30: Anti-Vn mAb competitive ELISA. 85
Figure 31: Size-exclusion HPLC analysis of Vn-1E9 complex formation. 87
Figure 32: Size-exclusion FPLC isolation of Vn-1E9 complex for crystallization screen. 89

LIST OF ABBREVIATIONS

ACES	N-(2-acetomido)-2 aminoethane sulfonic acid
AUC	Analytical ultracentrifugation
BSA	Bovine serum albumin
D-14-1B PAI-1	Perdeuterated 14-1B mutant plasminogen activator inhibitor type-1
ECM	Extracellular matrix
ELISA	Enzyme-linked immunosorbent assay
EPR	Electron paramagnetic resonance
FPLC	Fast protein liquid chromatography
HEPES	4-(2-hydroxyethyl)piperazine-1 ethanesulfonic acid
HPLC	High-performance liquid chromatography
IPTG	Isopropylthiogalactoside
kDa	Kilodalton
LB	Luria broth
mAb	Monoclonal antibody
MAC	Membrane attack complex
MES	Morpholinoethane sulfonic acid
MOPS	3-(N-Morpholine-)propane sulfonic acid
NTA	Nitriloacetate
PAI-1	Plasminogen activator inhibitor type 1
PBS	Phosphate buffered saline
RCL	Reactive center loop
RGD	arginine-glycine-aspartate sequence
SANS	Small-angle neutron scattering
SAXS	Small-angle x-ray scattering
SDS-PAGE	Sodium dodecyl sulfate polyacrylamide gel electrophoresis
Serpin	Serine protease inhibitor
SMB	Somatomedin B
SSF	Serum spreading factor
TBS	Tris buffered saline
tPA	Tissue-type plasminogen activator
uPA	Urokinase-type plasminogen activator
uPAR	Urokinase receptor
Vn	Vitronectin

CHAPTER 1

INTRODUCTION TO VITRONECTIN AND PLASMINOGEN ACTIVATOR INHIBITOR TYPE 1; STATEMENT OF RESEARCH OBJECTIVES

Introduction

Overview of Vitronectin

Vitronectin is a multi-domain, adhesive glycoprotein found in both the extracellular matrix (ECM) [1] and plasma, where it circulates at a relatively high concentration (micromolar range) [2,3]. It is involved in regulation of such physiological processes as coagulation, wound healing, tissue remodeling, angiogenesis, and the complement-mediated cellular immune response. To facilitate participation in these varied processes, vitronectin is able to bind to many and varied ligands, including heparin, plasminogen activator inhibitor-type I (PAI-1), complement components, cell surface receptors and integrins [4,5]. The 459 amino acids of vitronectin include side chains which are glycosylated, sulfated, or phosphorylated. The glycosylations, along with the 62-kDa molecular weight of this protein and its tendency to self-multimerize, make three-dimensional structural studies of the protein particularly challenging. High-resolution structural information for vitronectin is limited to the somatomedin B (SMB) domain (the N-terminal 44 residues of vitronectin): solution structures were established by NMR on both the human plasma-purified domain (2.29 Å resolution for core region) [6] and a recombinant SMB domain [7]; a crystal structure was solved for another recombinant SMB domain in complex with a key vitronectin-binding protein, (PAI-1) (2.3 Å

resolution) [8]. In addition, a low-resolution model of vitronectin from small-angle x-ray scattering (SAXS) [9] and computational models using a threading algorithm for three main domains of vitronectin (see Figure 1) [10] have been published by this laboratory. The SAXS model indicates the shape of vitronectin to be oblong and bi-lobed, somewhat like that of a peanut (see Figure 2).

The primary sequence of vitronectin can be divided into three main domains plus a connecting region: the aforementioned N-terminal SMB domain, the connecting region, a central hemopexin homology domain, and a C-terminal heparin-binding domain [11]. As a regulatory protein, vitronectin executes its many functions by binding to its various ligands. Many of these binding interactions have been localized to one of the main domains. Figure 3 shows the linear domain arrangement of vitronectin together with key ligand binding locations. Details of each domain are given in the following section.

Domain Structure of Vitronectin

The 44-residue SMB domain shares primary sequence with somatomedin B, a peptide of unknown function present in the circulation [11]. Within this compact, 5-kDa domain is a network of four disulfide bonds, whose pairings remain controversial. Through limited proteolysis, CNBr cleavage, acid cleavage, and peptide mapping, our laboratory proposed one arrangement [12], but two other groups have proposed different arrangements [8,13]. While the proposal from our lab came from analysis of SMB domain cleaved and isolated from human plasma vitronectin, the others came from working with recombinant forms of SMB produced in *E. coli.* The latter means of obtaining the peptide leads to questions of whether correct folding and disulfide pairing occurred when expressed in a prokaryote.

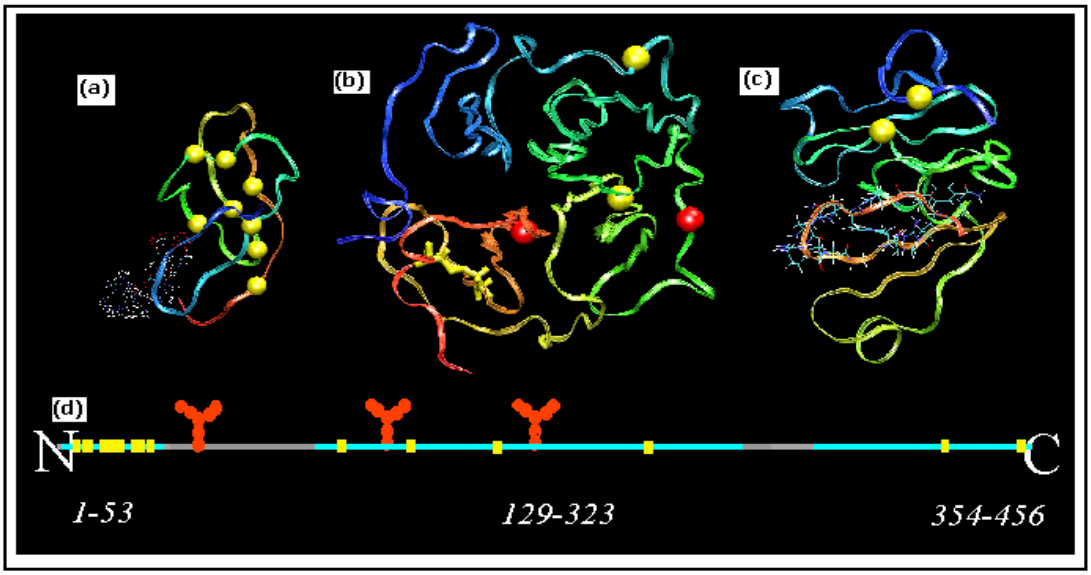


Figure 1: Domain structure predictions for vitronectin obtained from sequence-structure alignment and fold recognition (threading).
a, SMB domain; *b*, central hemopexin homology domain; *c*, C-terminal heparin binding domain; *d*, linear primary sequence representation. *Yellow bars* and *spheres* represent cys residues. *Red circles* and *spheres* represent glycosylations. Figure from Ref. [10].

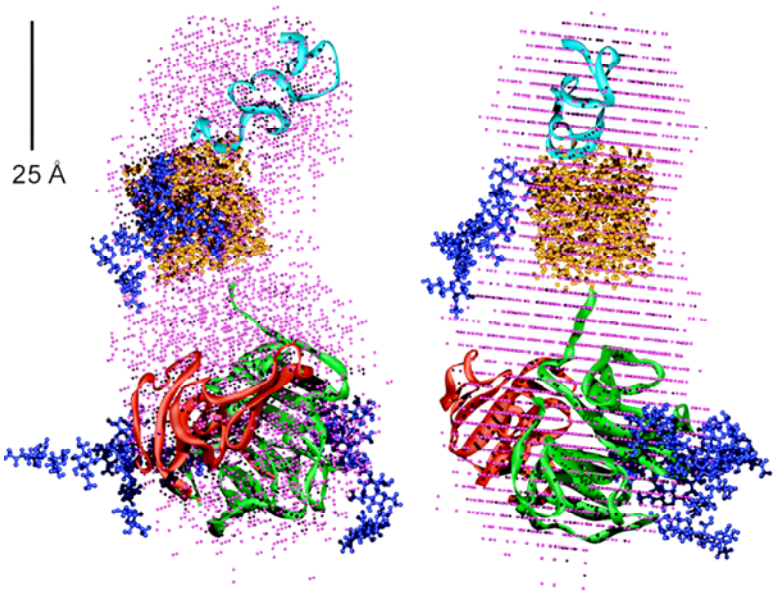


Figure 2: SAXS Model of Vitronectin.
The purple dots represent the consensus envelope for the protein obtained from SAXS data, onto which a model assembled from domain structures together with SAXS data was overlaid [9]. The blue ribbon structure near the top is the NMR structure of the SMB domain [6]. The green and red structures are the central and C-terminal domains, respectively, predicted from threading [10]. The orange structure near the center represents a cylindrical model for the connecting region. The two views are orthogonal rotations.

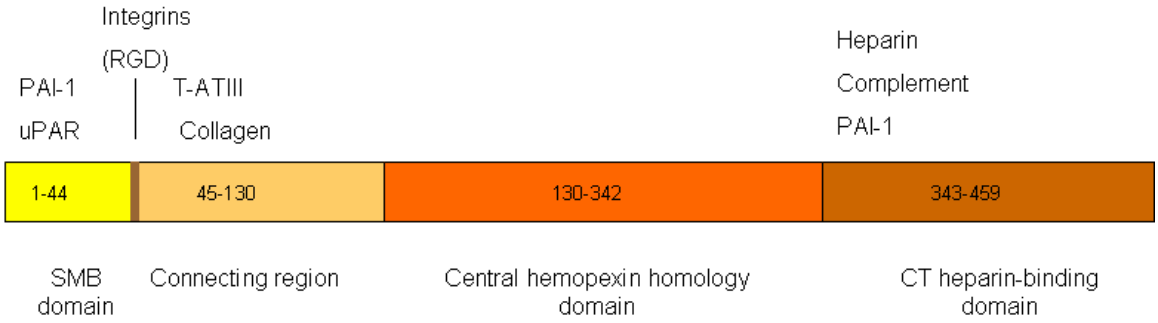


Figure 3: Vitronectin domains and locations of key ligand binding sites.
The linear sequence of vitronectin can be divided into three main domains plus a connecting region. The protein executes its regulatory functions by binding to a wide array of ligands. The domain locations of key ligand binding sites are indicated above each domain in the figure.

The primary binding site for PAI-1 is in the SMB domain, as is that for the urokinase-type plasminogen activator receptor (uPAR). From the NMR structure of the SMB domain (Figure 4), it can be seen to represent a unique fold, having little secondary structure, with the exception of the single-turn α-helix [6]. Residues 24 – 30, which include this helix, have been identified through mutagenesis work and the use of monoclonal antibodies as the site of PAI-1 binding [14].

Immediately following the SMB domain is the integrin binding sequence, arginine-glycine-aspartate (RGD). This sequence mediates cell adhesion by vitronectin [15-17]. The connecting region, spanning from residue 45 at the start of the RGD sequence, to residue 130, tethers the SMB domain to the central hemopexin-homology domain. This region is predicted to be unstructured [10]. It also houses binding sites for collagen, for interaction with the ECM, and the thrombin-antithrombin complex.

The central hemopexin homology domain is the largest, covering residues 131-342, and sharing significant sequence homology with hemopexin [18]. Hemopexin domains in proteins have been shown to produce the β-propeller fold [19], which is implicated in protein-protein interactions, as in the metalloprotein, collagenase [20]. Not surprisingly, structure predictions by threading predict with high confidence that the four hemopexin repeats of this domain are folded into a four-bladed β-propeller [10].

The C-terminal heparin-binding domain extends from residue 343 to 459. The N-terminal end of this domain begins with three additional hemopexin repeats, which are predicted to form only two blades of a β-propeller [10]. Following these repeats, a cluster of positively charged amino acids comprise the heparin binding site, which supports interaction with another key vitronectin ligand. Through heparin binding, vitronectin

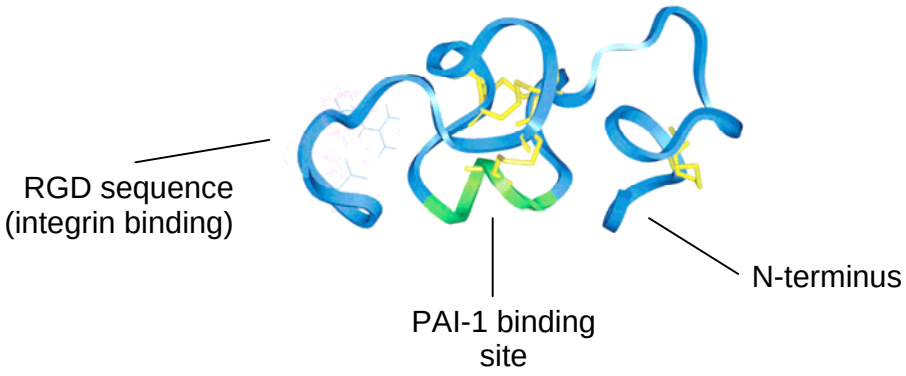


Figure 4: NMR Solution structure of the SMB domain of vitronectin.
The only secondary structural element of the compact SMB domain is a single-turn α-helix (shown in *green*), which is the site of PAI-1 binding. The four disulfide bonds are shown in *yellow*. The peptide used for this structure includes the RGD sequence just past the C-terminus of the SMB domain; this sequence mediates cell binding of vitronectin through integrins. Adapted from [6].

regulates hemostasis by affecting the thrombin-antithrombin interaction. Vitronectin competes with thrombin and antithrombin for heparin binding [21]. Without heparin, antithrombin is less effective at inhibiting thrombin, which is free to initiate blood clotting.

Another collagen binding site is in this domain, as well as the site of complement component interaction. Secondary PAI-1 and uPAR binding sites may exist in the C-terminal domain, but their existence has been controversial. Recently, work from our laboratory using an SMB-deletion mutant of vitronectin has shown the persistence of PAI-1 binding in the absence of the SMB binding site [22]. This is strong evidence in support of the second PAI-1 binding site. However, this work also shows abolition of uPAR binding upon deletion of the N-terminal uPAR binding site, indicating that no secondary uPAR binding site exists outside the SMB domain of vitronectin.

Overview of PAI-1

PAI-1 is a member of the serine protease inhibitor (serpin) superfamily of proteins. As one of many binding partners of vitronectin, PAI-1 is found in the circulation and in the ECM. It functions as a regulator of clot formation and fibrinolysis, by inhibiting cleavage of plasminogen to active plasmin, which proteolyzes fibrin.

The protein now known as PAI-1 was first described in 1984, as an unknown inhibitor of plasminogen activators present in human serum [23]. This type of inhibition was new to researchers, as it indicated a point of regulation of fibrinolysis earlier than occurs for the active proteases, such as the well-known antiplasmin. It was suggested this protein represented a new class of inhibitors, termed the “antiactivators.”

Within a few years, an unknown binding protein of PAI-1 was detected in plasma, present in high molecular weight complexes [24,25]. This protein was isolated and identified as S-protein, or vitronectin [26], and was shown to increase the half-life of the labile PAI-1 at 37°C by 2-3-fold, compared to purified PAI-1. It was proposed that vitronectin may stabilize PAI-1 in the blood as well. Indeed, it is now known that circulating PAI-1 is almost exclusively bound to vitronectin [26].

As a serpin, PAI-1 shares structural similarity to other family members, such as antithrombin, but it is unique in its short half-life of approximately 90 min. Through a spontaneous conformational change, active PAI-1 is converted to an inactive, latent form [27]. It is probable that this structural lability contributes to the regulatory function of the protein. Key structural features of PAI-1 are a central β-sheet (β-sheet A), nine α-helices (hA-hI), and a reactive center loop (RCL) extending away from the protein (see Figure 5).

The serpin mechanism of inhibition involves the flexible RCL, containing the recognition sequence of the target serine protease, which can bind to the RCL and begin the process of substrate cleavage via the catalytic triad. However, once the peptide bond is cut, while the enzyme is covalently bound to the serpin as an acyl-enzyme intermediate, the cleaved RCL translocates and inserts as a sixth strand in the central β-sheet, taking the trapped protease with it. This disrupts the active site of the enzyme such that it cannot complete the cleavage mechanism to release itself from the inhibitor. The same mode of RCL insertion into β-sheet A is the mechanism by which active PAI-1 converts to the latent form, which is an energetically more favorable conformation [28].

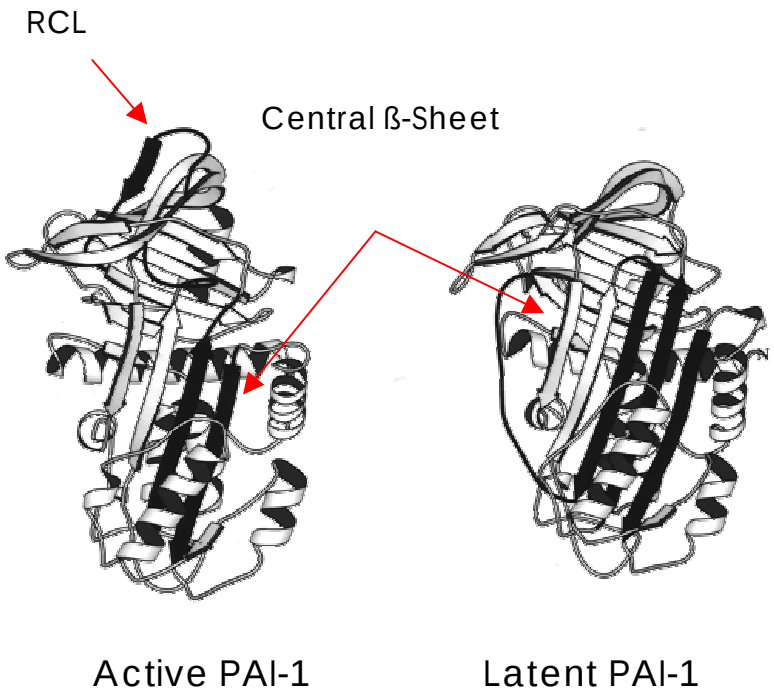


Figure 5: Active and latent forms of PAI-1.
In active PAI-1, the RCL is extended as a target for a serine protease. PAI-1 readily converts to an inactive, latent form, by insertion of the RCL into the β-sheet. Adapted from [27].

The x-ray crystal structure of the SMB domain of vitronectin in complex with PAI-1 helped elucidate how vitronectin stabilizes PAI-1 in its active conformation [8]. The primary vitronectin binding site is located at the base of β-sheet A, near the opposite end of the protein from the extended RCL. Here, through interaction with both hE and hF, vitronectin obstructs β-sheet A from opening to allow RCL insertion. Thus, the RCL remains solvent-exposed and available as a target for proteases.

Recently, attention has been given to mapping a secondary vitronectin binding site on PAI-1. Since the primary site involves interaction with the SMB domain, our laboratory engineered a recombinant SMB-deletion mutant vitronectin for studies of the secondary PAI-1 binding site on vitronectin as well as a complementary site on PAI-1 [22,29]. Using a variety of PAI-1 mutants, and surface plasmon resonance (SPR) experiments, a region of residues involved in binding to vitronectin outside the SMB domain was identified. This region is near, but separate from, the region that binds to the SMB domain.

The functions of both vitronectin and PAI-1 are affected by their mutual interaction. Vitronectin stabilizes PAI-1 in its active conformation, and PAI-1 causes vitronectin to multimerize. Multimeric vitronectin is deposited in the ECM, where vitronectin mediates its cell adhesion effects. In this way, PAI-1 helps localize vitronectin from the plasma to areas of injury or inflammation to regulate hemostasis.

What lines of research led to our current understanding of vitronectin? How did this understanding develop? What were the key early discoveries and areas of contention?

Development of Thought on Vitronectin: A Story of Convergent Experimental Paths

Beginnings of the cell adhesion path of study

A driving force in cell biology research in the mid-20th century was the quest to identify components necessary to support mammalian cell growth in serum-free medium. By 1955, Eagle had catalogued amino-acid and vitamin requirements for many cell types[30], but most cultures still had to be supplemented with at least 5% serum. This was acceptable for some experiments, but in other cases, the complex and indeterminate components of serum led to difficulty interpreting experimental results [31]. More than a decade later, Holmes described his "α-1 protein" from human serum, having studied its positive effect on cell growth and morphology, after partial purification on glass beads [32]. Years would pass before this protein would be isolated and called vitronectin. However, in light of current knowledge that vitronectin is rather difficult to isolate and work with, it is understandable that optimism over the potential benefits of such a protein growth factor was not soon followed by reports of successful exploitation in cell culture.

So sought-after was the identification of growth factors in serum, that a peptide found in the circulation was prematurely given the name "somatomedin B" (SMB) to highlight its proposed role as a somatotropin-dependent mediator of cell growth [33]. In 1978 Fryklund and Sievertsson published the primary structure of the SMB peptide [34], information that eventually would prove useful in the study of vitronectin. A few years later, however, the same group that initially identified SMB established that the

mitogenic activity attributed to it was actually due to contaminating epidermal growth factor [35]. Yet, the name of the peptide remains today, as does the mystery of its purpose.

Beginnings of the complement system path of study

The protein now known as vitronectin next appears in the literature on its other path of early study. Kolb and Muller-Eberhard, investigating complement components in serum, detected an unknown protein in the C5b-9 complex, also known as the membrane attack complex (MAC) of complement [36]. Several reports combined to elucidate the function of this protein in binding to the precursor C5b-7 complex, to maintain complex solubility as complement components C8 and C9 are added; the resultant soluble MAC is unable to insert into cell membranes for lysis (as the normally amphiphilic MAC does) [37-40]. Thus, this protein protects cells from complement-induced destruction; the name "S-protein" is meant to reflect its competition with membrane sites for binding to the MAC [37]. Now interest in this "newly identified" protein was sufficient to warrant development of effective purification procedures, some of which are still the basis of protocols used today to isolate native, monomeric vitronectin [41,42]. Development of these procedures was neither quick nor trivial, as S-protein was noted to have a "tendency to aggregate and adsorb to various surfaces," resulting in quite low yields from early isolation attempts [43].

Because S-protein was found in the serum and active in the complement system, researchers looked for its involvement also in the coagulation system, as a potential regulator of hemostasis. S-protein was found in ternary complex with the serine protease, thrombin, and its inhibitor, antithrombin-III [44].

Advances in the cell adhesion path of study

While several groups were busy characterizing S-protein from the perspective of involvement in the complement and coagulation systems, Barnes and coworkers, on the cell adhesion path of investigation, coined the term "serum spreading factor" (SSF) to describe partially isolated serum protein [31,45]. They showed that, for a human mammary tumor cell line, SSF supports not only the same cell growth rate as does serum, but also the same spreading morphology – a morphology similar to that reported by Holmes [32,45]. The activity of the protein, together with the observation of similar electrophoretic patterns, led to the conclusion that their SSF and Holmes' α-1 protein are the same. Contemporary studies by Knox and Griffiths [46] and Knox and Whateley [47] provided similar evidence of the adhesive, spreading, and growth effects of this protein on cultured cells.

Skeptics were suspicious that this newly discovered protein was merely fibronectin or a fragment thereof. While both proteins do contribute to cell adhesion, spreading and growth, investigators offered much evidence that SSF was a unique protein, unrelated to fibronectin [45,46,48]. For example, fibronectin antibodies blocked cell adhesion to fibronectin but not SSF [49]; conversely, SSF antibodies blocked spreading activity of SSF but not of fibronectin [50]; and no fibronectin homology was found from examination of N-terminal residues of multiple CNBr fragments of SSF [11].

The same reasoning that lead to skepticism about the uniqueness of SSF, also provided inspiration for new SSF studies. Tissues that were known to harbor fibronectin were probed for SSF. Soon the protein was found to exist not only in the circulation, but also in the ECM of many tissues and on cell surfaces, distributed similarly to fibronectin,

but having intensities clearly distinct from those of fibronectin [1]. Once the adhesive properties of SSF in the ECM had been described, expanding the realm of the protein past the serum, the less-restrictive moniker "vitronectin" was proposed, harkening back to Holmes' single-step isolation on glass beads [1].

Similarly to fibronectin, vitronectin was shown to be arranged in functional domains along the length of its primary structure [11]. Sequencing of the first 30 N-terminal residues led to the surprising discovery that this part of the protein was identical to the somatomedin B peptide identified several years earlier [33,34]. Also in this study, peptide mapping using CNBr fragments provided evidence that the cell-binding site is near the N-terminus but outside the SMB domain; soon the same group determined that the cell-binding site is the RGD sequence, the same as that of fibronectin [15]. A heparin binding region was mapped to a 12-kDa fragment near the C-terminus of the protein. This fragment was the only one found to bind to heparin-sepharose [11]. From alignments of the sequenced N-termini of the CNBr fragments used in the study, this heparin-binding region was shown to be rich in basic amino acids, well suited to interaction with the negatively charged heparin molecule.

Further advances were made as several groups developed monoclonal antibodies to vitronectin, for use in both immunoaffinity purification and probing samples for anti-vitronectin reactivity, as in the tissue study mentioned above [1,50]. In another example, platelet extracts were shown to have anti-SSF binding activity, while erythrocytes do not [50].

Two early purification schemes which were independently developed for SSF showed apparently contradicting heparin-binding properties of the protein at physiological ionic

strength and pH. Heparin-affinity chromatography was a logical purification step, due to the presence in plasma of heparin and multiple heparin-binding molecules; fractionation by heparin interaction would result in SSF enrichment of either the bound or the unbound portion of the sample. In the method of Barnes and Silnutzer, SSF was bound to heparin-sepharose by loading in 0.1 M NaCl at pH 6.0; the protein was eluted by raising the pH to 7.2, near physiological [2]. In the method of Ruoslahti's laboratory, SSF was bound to heparin-sepharose by loading in PBS, and eluted at the high salt concentration of 0.5 M NaCl [1]. After this report, the former group noted that the heparin-affinity step in Ruoslahti's method followed elution from an immunoaffinity column with "potentially denaturing" 8M urea [51]. Speculating that this difference in isolation procedures led to the apparent contradiction in whether SSF can bind heparin under physiological conditions, they performed a set of experiments to test this idea. They found that exposure of SSF to denaturing treatments of either urea, heat, or acid, does result in heparin-binding activity at physiological ionic strength and pH; but for native SSF under physiological conditions – even in unfractionated plasma – only 25% of the protein exhibits heparin-binding activity [51]. This result was confirmed later in a study by Hogasen *et al.* [52] related to complex formation in the complement system.

In 1985, Hayashi *et al*. – using a denaturing step in their purification of vitronectin – proposed the "cryptic-to-open" model to explain the heparin-binding disparities documented for vitronectin [53]. This model contends that the heparin site in native vitronectin is concealed, and is exposed only upon a conformational change, such as results from denaturation. Curiously, this conclusion was reached after assessing heparin

affinity only by column chromatography, without any supporting experiments in solution or by alternative means of heparin immobilization.

As a means of explanation for the differences observed in heparin-binding activity of vitronectin, this model (also known as the "cryptic-site" model) was generally accepted for many years, and even invoked to explain similar experimental results concerning collagen binding by vitronectin [54]. However, with the first binary solution testing of the vitronectin-heparin interaction, using a labeled heparin probe, work from our laboratory strongly supported an alternative explanation for the apparent increase in heparin affinity, involving the alteration of vitronectin to a multimeric form upon denaturation. The perceived increase in affinity is an effect of one heparin molecule being able to interact with more than one binding site on adjacent molecules of denatured – and multimeric – vitronectin [55].

Convergence of the two paths

In a seminal paper in 1985 by Jenne and Stanley, who had been working to clone S-protein from cDNA for studies of its involvement in the complement system, the authors deduce that S-protein and vitronectin are the same protein [56]. In reaching this conclusion, which was not even a speculation at the outset of their work, they assimilated many clues. The primary clue came from a database search using the newly deduced amino acid sequence of S-protein. The N-terminal sequence matched that of the SMB peptide, which had also recently been identified as the N-terminal of SSF [11], also known as vitronectin by then. Further searching of the SSF literature provided additional evidence: partial peptide sequences from SSF coincided with residues in their sequence [11]; the amino acid compositions by percentages were very similar [2]; and multiple-

banded electrophoretic patterns from SDS-PAGE, from several laboratories, were similar [1,11,41,43].

Importantly, the identity of these two proteins revealed connections among the complement defense system, the coagulation cascade, and cell-substrate adhesion. The body of knowledge of each "separate" protein was instantly expanded to incorporate that of the "other" protein. Monoclonal antibodies could be shared; isolation procedures could be compared, combined, and optimized; assays could find new applications.

Coincidentally, while the Jenne and Stanley paper was in press, the cDNA sequence for SSF/Vn was published [15], but with no recognition of the identity with S-protein. However, these authors did not have access to even partial sequence information for S-protein.

Also at this time, another group was actively seeking evidence in the literature of an alternate description of the SSF/Vn protein, reasoning that its high plasma concentration may have led to its earlier discovery and characterization, yet by a different name [57]. This line of thought led them to study S-protein. They not only cite literature evidence, but also support the idea by several of their own experiments, including S-protein mAb inhibition of fibroblast spreading and SSF/Vn mAb reactivity with complement-activated serum. The two papers reporting the cDNA sequences appeared during the preparation of their work for submission and while in press. However, theirs was the first experimental evidence that SSF/Vn and S-protein are the same protein, and this evidence solidified the argument.

The early shared path: A rocky road

Once researchers from different areas of study learned that they were studying the same protein, opposing views on the function of the protein quickly followed. The lability and self-aggregating tendency of vitronectin make interpretation of experimental results challenging and often ambiguous. In fact, not everyone embraced the greatly widened body of knowledge on "their" protein provided by research on the "other" protein.

As an example, one researcher of complement and S-protein even suggested that the cell adhesion and spreading activities reported for SSF were artifacts of the assay system used [18]. The same study showed the primary structural homology of vitronectin with hemopexin, and it was proposed that vitronectin might, therefore, have a scavenging function for terminal components of the complement and coagulation systems. Calling heparin the "priniciple ligand" of vitronectin, and placing the protein in the pexin family due to the large proportion of its sequence taken up by hemopexin repeats, this paper proposed yet a fourth name for the protein: heparopexin. However, the scavenging function, while a logical proposal, was not to be supported experimentally. Vitronectin is now classified among other proteins, including metalloproteins such as collagenases and gelatinases, which bear hemopexin domains but are functionally unrelated to hemopexin [20]. Instead, as described above, the hemopexin domain has been shown to produce the β-propeller fold [19], which is implicated in protein-protein interactions [20]. Our laboratory is currently investigating whether this domain in vitronectin is involved in the self-mulitmerization of the protein.

Questions regarding the functions and interactions of vitronectin and PAI-1

Because vitronectin and PAI-1 are both involved in such a wide range of processes, the field of study of these two proteins is quite broad. Questions of interest for this work are centered on the functional and structural effects that vitronectin and PAI-1 exert upon each other through their interaction. What conformational changes occur in vitronectin when PAI-1 binds to it? How do these changes lead to multimerization of vitronectin? Do metal ions affect the interaction or function of vitronectin and PAI-1? The work presented here aims to probe the structural and functional aspects of vitronectin and PAI-1, to aid in development of a more detailed picture of the interaction between these two regulatory proteins.

Research Objectives

The work presented in this thesis involves three projects designed to probe structural and functional aspects of vitronectin and PAI-1. The aims of these projects are given below, while the projects and their results are described in Chapters 2, 3, and 4. Specific aim 1 is addressed by the first project; specific aims 2a and 2b are addressed by the second and third projects, respectively.

Specific Aim 1

Characterize metal binding by vitronectin, PAI-1, and the vitronectin-PAI-1 complex.

Aim 1a: Use EPR spectroscopy to test for metal binding by vitronectin, PAI-1, and the vitronectin-PAI-1 complex.

Aim 1b: Determine the effect of metals on the activity of vitronectin and PAI-1.

Specific Aim 2

Develop reagents for use in structural studies of vitronectin.

Aim 2a: Express, purify, and confirm activity of deuterated PAI-1, to be used in complex with vitronectin in future neutron scattering experiments.

Aim 2b: Characterize several monoclonal antibodies to vitronectin to identify their interaction with monomeric and multimeric vitronectin, and the vitronectin-PAI-1 complex. Identify candidate antibody(ies) for crystallization screens in complex with vitronectin.

CHAPTER 2

CHARACTERIZATION OF VITRONECTIN AND PAI-1 METAL BINDING

Introduction

Evidence of Metal Binding

Based on evidence that both vitronectin and PAI-1 bind metals, we hypothesized that both PAI-1 activity and interaction of vitronectin with PAI-1 are affected by metals. Such evidence of metal-binding includes the observation that metal added to vitronectin causes the protein to migrate differently on a polyacrylamide gel (Ze'ev Gechtman, personal communication). Metals affect binding of integrins by vitronectin, as shown by elimination of binding of the vitronectin/PAI-1 complex to integrin GPIIbIIIa, in the presence of EDTA [58]. Also, $Mg^{2+}$and Ca^{2+} are required components of the integrin-binding buffer used for vitronectin-integrin binding assays in our laboratory, as omission causes spurious outcomes of binding experiments (Sumit Goswami, personal communication). Furthermore, both vitronectin and PAI-1 are involved in altering the ECM, where metals are known to be important.

Metals also influence the purification of recombinant PAI-1; our laboratory uses an immobilized nickel-NTA column to bind PAI-1 (without a His-tag) during purification. Using immobilized metal affinity chromatography (IMAC), a collaborator and supplier of recombinant PAI-1 has demonstrated that PAI-1 binds to immobilized Co^{2+}, Cu^{2+}, Mn^{2+}, Ni^{2+}, and Zn^{2+}, as shown by the elution profile data represented in Figure 6 (Ingrid

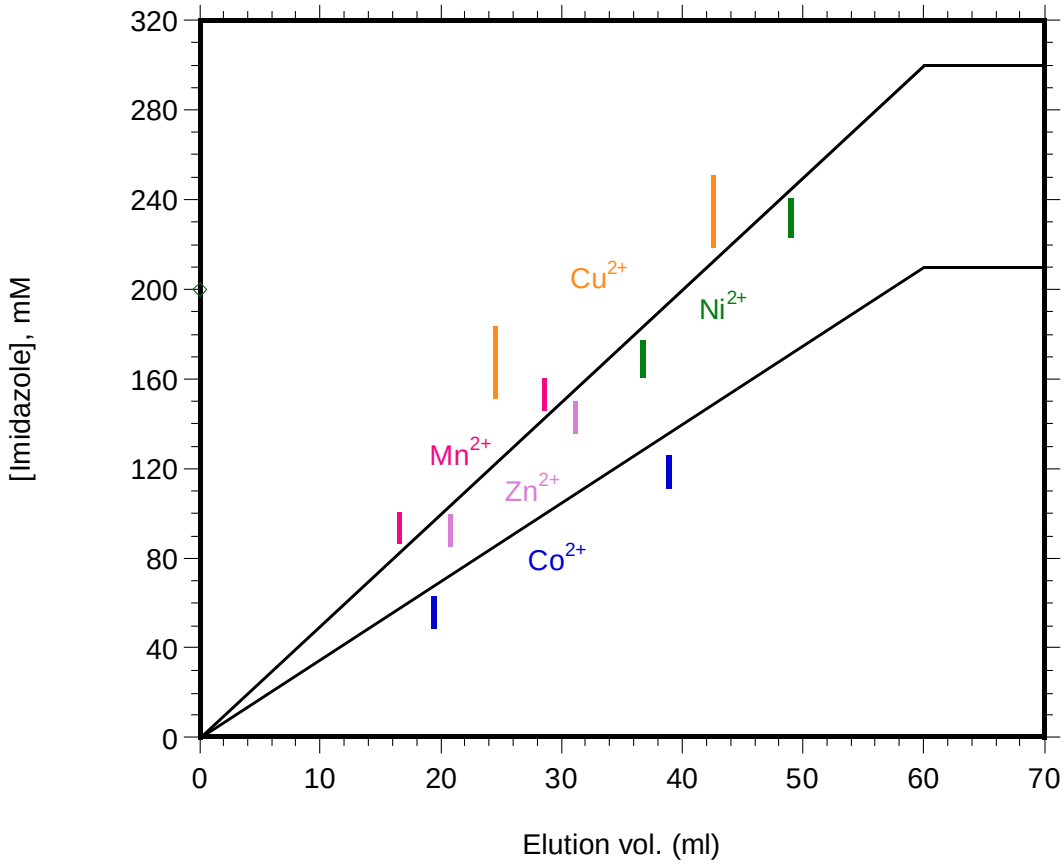


Figure 6: Composite elution profile for PAI-1 bound to five metal-affinity columns. Five affinity columns, each charged with a different metal (Co^{2+}, Cu^{2+}, Mn^{2+}, Ni^{2+}, or Zn^{2+}) were loaded with a bacterial cell lysate containing PAI-1. Bound PAI-1 was eluted with an imidazole gradient (either 0–210 mM imidazole or 0–300 mM imidazole). The *y-axis* shows the concentration of imidazole in the gradients, while the *x-axis* indicates the volume of eluate collected. The *vertical lines* around a metal indicate the imidazole concentration range at which PAI-1 eluted from the corresponding metal-charged resin. Metals requiring a higher imidazole concentration for PAI-1 elution are regarded as binding PAI-1 more tightly than metals requiring a lower imidazole concentration for PAI-1 elution. (Data provided by Ingrid Verhamme and Duane Day, Molecular Innovations, Inc.)

Verhamme and Duane Day, Molecular Innovations, Inc., personal communication). These data give qualitative, but not quantitative, relative binding "affinities," based on the concentration of imidazole required to elute the bound protein from each metal affinity column. Metals requiring a higher imidazole concentration for PAI-1 elution are regarded as binding PAI-1 more tightly than metals requiring a lower imidazole concentration for PAI-1 elution.

Site-directed mutagenesis work with PAI-1 by a collaborator (Duane Day, Molecular Innovations, Inc., personal communication) has provided evidence of a potential metal-binding site on PAI-1. Whereas wild-type human PAI-1 (hPAI-1) binds to the TALON Co^{2+} affinity resin, the mutant, R76E hPAI-1, loses this ability. Residue R76 is located in a region of positively charged amino acids, near the secondary vitronectin-binding site on PAI-1, as indicated in Figure 7. Supporting the notion that R76 is part of a metal-binding site is the observation that neither mouse PAI-1 (mPAI-1) nor rat PAI-1 (rPAI-1) binds to TALON resin, and neither of these has an arginine at position 76. However, rabbit PAI-1, which does have arginine at residue 76, does bind TALON resin.

Mutations to mPAI-1 in the region near residue 76 have been observed to induce TALON binding in this species. K115R mPAI-1 exhibits partial TALON binding, while K115R / Q77H mPAI-1 exhibits full TALON binding. The locations of these residues are indicated in Figure 7. It is noteworthy that both of these mutations involve replacement of a positively charged amino acid with either another positively charged amino acid (K115R) or an uncharged (at physiological pH) amino acid (Q77H). R76E hPAI-1, which loses TALON binding, also involves replacement of a positively charged residue with another positively charged residue. In other words, no charge reversal among these

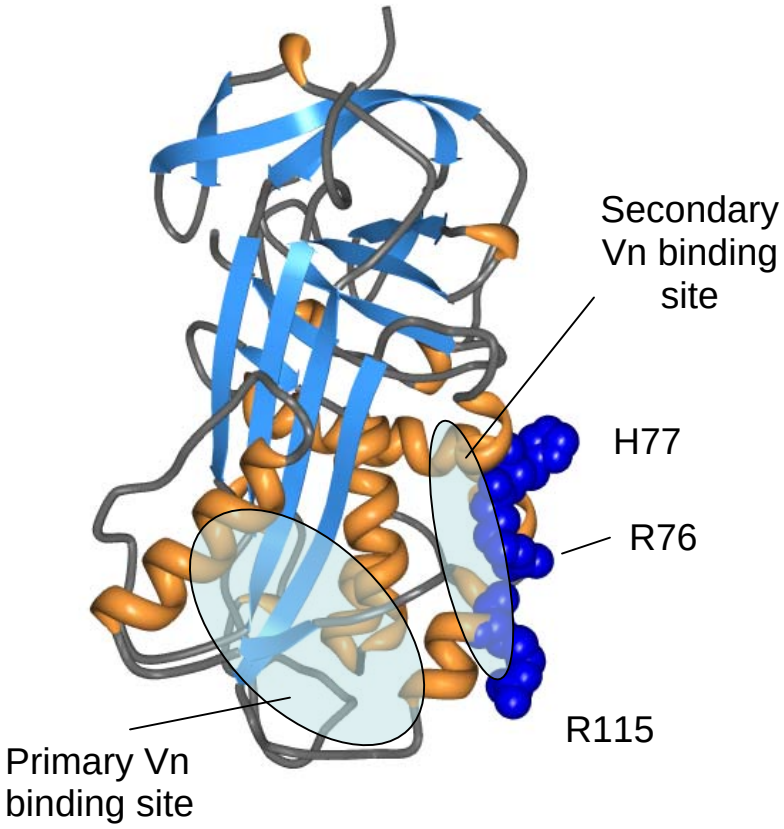


Figure 7: Putative metal-binding site on PAI-1.
In this structure of PAI-1 (PDB accession file 1OC0), three residues determined by mutagenesis to be involved in metal binding are colored *blue*. The regions of the primary and secondary binding sites for Vn are indicated with *ovals*. Figure was rendered using the Molecular Biology Toolkit [59].

residues is necessary to alter PAI-1 binding to the TALON Co^{2+} affinity resin. Furthermore, R76 and the mutated arginine at position 115 (which partially restores metal binding), as well as metal ions, are all positively charged. Therefore, direct charge-charge interaction of key PAI-1 residues and metal ions does not appear to mediate metal binding by the protein. It is possible that second-sphere complexes involving water molecules mediate PAI-1 metal binding instead. Based on the evidence of PAI-1 metal binding, together with the preceding evidence of vitronectin metal binding, we chose to characterize metal binding by both proteins, as well as their complex.

Electron Paramagnetic Resonance Studies

We used electron paramagnetic resonance (EPR) to test for metal binding by each protein separately, and by the complex formed between vitronectin and PAI-1. EPR is a spectroscopic technique that detects species that have unpaired electrons. Examples of metals with unpaired electrons are Mn^{2+}, Cu^{2+} and Co^{2+}, while Mg^{2+}, Ca^{2+}, Zn^{2+} and Ni^{2+} are examples of metals without unpaired electrons. Unpaired electrons can be induced to align – either parallel or antiparallel – to an external magnetic field, making the material temporarily magnetic. This property is known as paramagnetism. EPR is similar to NMR spectroscopy, in that an applied magnetic field is used to induce subatomic particle transitions that can be detected and used to characterize a sample. Whereas NMR detects nuclear transitions, EPR detects unpaired electron transitions. EPR can be applied to study metal binding by macromolecules such as proteins. The spectrum of the free metal alone in solution can be compared to the spectrum of the metal in solution with a protein. If the protein binds the metal, the signal decreases because the metal is bound to the much larger protein molecule. The resulting spectrum will reflect the fraction of free

metal remaining. Thus, changes in paramagnetic spectra provide evidence of metal binding by proteins.

We chose Mn^{2+} and Cu^{2+} for our metal-binding studies. These metals are two of the three paramagnetic metals observed to have PAI-1 affinity in IMAC, as described above. The third paramagnetic metal, Co^{2+}, was rejected from consideration because its short correlation time necessitates liquid nitrogen temperature to acquire an EPR spectrum, and we do not have access to the equipment for such experimental conditions. Conversely, Mn^{2+} has the longest correlation time among the three paramagnetic metals, allowing acquisition of useful EPR spectra at room temperature. Therefore, Mn^{2+} was an attractive choice for our studies. Cu^{2+} was chosen because it was observed to bind PAI-1 more tightly than Mn^{2+}, Co^{2+}, or Zn^{2+} in IMAC; only the Ni^{2+} affinity column required a higher concentration of imidazole to elute bound PAI-1. Although more Cu^{2+} EPR spectra in the literature were acquired at liquid nitrogen temperature (see *e.g.* [60] and [61]), rather than room temperature, we anticipated PAI-1 to bind Cu^{2+} tightly enough to permit detection of binding using room-temperature spectra. In addition, we planned first to confirm the validity of using EPR to detect Cu^{2+} binding to a protein, by acquiring and comparing Cu^{2+} spectra in the presence and absence of bovine serum albumin (BSA), a protein known to bind Cu^{2+}.

BSA has a high-affinity Cu^{2+}-binding site at its N-terminus, with a Kd of controversial value, but estimated to be as high as 10^{-12} to 10^{-13} M [62]. A recent report on human serum albumin, which has the same X-Y-His metal-binding motif at its N-terminus, used competitive UV-vis spectroscopy titrations to determine the Cu^{2+}-binding affinity of this site to be 1 pM at pH 7.4 [63]. A second Cu^{2+}-binding site on BSA has

been estimated to have micromolar affinity [62]; this site is also termed the "multi-metal binding site" because Ni^{2+}, Zn^{2+}, and Cd^{2+} can compete for binding here [64]. Three additional specific, lower-affinity Cu^{2+}-binding sites have been shown to exist in BSA [62]. Therefore, the study of Cu^{2+}-binding by BSA was deemed appropriate as a test of the validity of the use of EPR to characterize Cu^{2+}-binding by our proteins.

Our experimental strategy for metal-binding studies of PAI-1 and vitronectin was titration of each protein, and the complex of both proteins, with a range of Mn^{2+} or Cu^{2+} concentrations, to determine the resulting concentrations of free Mn^{2+} or Cu^{2+}. We used Scatchard analysis to estimate binding stoichiometry and a dissociation constant.

Kinetic Assay for PAI-1 Activity and Stability

To test for an effect of metals on PAI-1 activity, as well as test for an effect on stabilization of PAI-1 by vitronectin, we used a kinetic assay. This assay employs a chromogenic substrate for trypsin, a serine protease; product formation can be monitored by an increase in absorbance of light of a particular wavelength. PAI-1 activity can be assessed by its ability to inhibit trypsin, resulting in less product formed and a lower end absorbance. Because of the inherent tendency of PAI-1 to convert to its inactive, latent form, we can use this assay to monitor loss of PAI-1 activity over time; we can then compare this trend to that observed for PAI-1 in the presence of metals. To test for a difference in the stabilizing effect that vitronectin normally has on PAI-1, we can perform the assay with vitronectin added to PAI-1, in the presence and absence of metals.

Materials and Methods

Materials

Native vitronectin from human plasma was isolated essentially as described by Dahlback and Podack [41], with modifications as in Bittorf, et al. [42]. Recombinant PAI-1 was either purchased from Molecular Innovations, or prepared with slight modifications to the method described in Chapter 3 of this work, using SP sepharose, Ni^{2+}-affinity, and SP-100 gel filtration chromatography for purification. BSA (Fraction V; heat-shock treated) and $MgCl_2$ were from Fisher Scientific. Bovine pancreatic trypsin and $CuSO_4$ were from Sigma; high-purity $MnCl_2$ was from Johnson Matthey. Sequencing grade trypsin was from Promega. PD-10 disposable desalting columns were from GE Healthcare.

Preparation of Protein for EPR Experiments

All protein manipulations were carried out at 4°C. For Cu^{2+}-binding studies with BSA, the protein was dissolved in 10 mM ACES buffer, pH 7.0, 0.5 mm EDTA (added to chelate potential trace metals in the preparation). To remove EDTA, along with any chelated metal ions, BSA was applied to a PD-10 desalting column equilibrated in 10 mM ACES buffer, pH 7.0. Protein-rich fractions were identified by absorbance at 280 nm, pooled, and concentrated in a 4-ml Amicon Ultra centrifugal filtration device (Millipore). Concentration was determined by absorbance at 280 nm in a Varian Cary Bio 50 UV-Visible spectrophotometer. For Mn^{2+}-binding studies with vitronectin, the protein was prepared from an $(NH_4)_2SO_4$ suspension; vitronectin was pelleted by centrifugation, resuspended in 25 mM Tris, pH 7.4, 0.15 M NaCl, 1 mM EDTA (added to chelate

potential trace metals in the preparation), and dialyzed into the same buffer without EDTA. To remove EDTA, along with any chelated metal ions, the protein was applied to a PD-10 desalting column equilibrated in 25 mM Tris, pH 7.4, 0.15 M NaCl; as described for BSA, protein-rich fractions were pooled and concentrated.

For Mn^{2+}-binding studies with PAI-1, which was stored at -80°C in either 50 mM sodium phosphate, pH 6.25, 0.30 M NaCl, 1 mM EDTA, or 50 mM sodium phosphate, pH 6.6, 0.1 M NaCl, 1 mM EDTA, the protein was diluted 1:1 or 1:2 into 200 mM Tris, pH 8.0, 0.15 M NaCl. This concentration and pH of Tris was necessary to minimize PAI-1 precipitation as the solution pH passed through the pI of PAI-1, which is 6.6. To remove any potentially precipitated protein after the dilution step, PAI-1 was centrifuged for 10 min and the supernatant transferred to a new microcentrifuge tube. This supernatant was applied to a PD-10 column equilibrated in 25 mM Tris, pH 7.4, 0.15 M NaCl, to exchange the buffer along with removing EDTA and any chelated metal ions. As described for BSA, protein-rich fractions were pooled, but PAI-1 was concentrated in a 0.5-ml Biomax Ultrafree centrifugal filtration device (Millipore). For Cu^{2+}-binding studies with PAI-1, protein was prepared in unbuffered 0.15 M NaCl, with a pH below 6.0. This solvent was used because all buffers tested either interacted with Cu^{2+}, or failed to maintain PAI-1 in a soluble state. The protein was diluted 1:1 into 0.15 M NaCl, then centrifuged and applied to a PD-10 column equilibrated in 0.15 M NaCl, to exchange the buffer along with removing EDTA and any chelated metal ions. Protein-rich fractions were pooled and concentrated in a 0.5-ml Biomax Ultrafree centrifugal filtration device.

EPR Spectroscopy

EPR experiments were performed with a Bruker EMX Spectrometer with an X-band microwave bridge, and WIN-EPR Acquisition Application software. Spectrum analysis was performed with Bruker WIN-EPR software. Instrument Settings: Instrument settings for Mn^{2+} studies were: modulation frequency = 100 kHz, modulation amplitude = 4.0 G, time constant = 163.8 ms, sweep time = 41.9 or 83.9 s, receiver gain = 2.0 x 10^5, microwave power = 6.82 or 21.6 mW, microwave frequency = 9.88 GHz. Instrument setting for Cu^{2+}-PAI-1 studies were: modulation frequency = 100 kHz, modulation amplitude = 4.9 G, time constant = 81.92 ms, sweep time = 5.24 s, receiver gain = 2.0 x 10^5, microwave power = 21.6 mW, microwave frequency = 9.88 GHz. Instrument settings for Cu^{2+}-BSA studies were: modulation frequency = 100 kHz, modulation amplitude = 4.9 G, time constant = 81.92 ms, sweep time = 10.8 s, receiver gain = 1.0 x 10^5 - 2.0 x 10^5, microwave power = 5.90 - 21.6 mW, microwave frequency = 9.88 GHz. Data Acquisition: All EPR spectra were acquired at room temperature. Sample volumes ranged from 70 to 90 μl. For an individual experiment, the protein concentration was held constant, while the metal ion was titrated into separate samples. For Cu^{2+}-BSA experiments and all Mn^{2+} experiments, each sample was mixed and allowed to incubate at room temperature for 1 – 2 min. immediately prior to loading in the instrument and acquiring a spectrum. For Cu^{2+}-PAI-1 experiments, because addition of Cu^{2+} often caused PAI-1 to precipitate, all samples were centrifuged to pellet any precipitated protein along with any bound Cu^{2+}. The supernatant was transferred to a new sample tube, and each supernatant was loaded into the spectrometer for spectrum acquisition. Data analysis: Before analysis of Cu^{2+} sample spectra, a baseline spectrum for a sample containing only

buffer was subtracted from the spectra for samples containing only Cu^{2+}; a spectrum for a sample containing only the protein was subtracted from the spectra for Cu^{2+}-protein samples. For Mn^{2+} samples, spectra were analyzed without subtraction of a baseline, because the peak heights were much greater than the noise.

Kinetic Assay for PAI-1 Activity and Stabilization by Vitronectin

The stability of PAI-1 in the presence of metal ions, as well as PAI-1 in complex with vitronectin in the presence of metal ions, was assessed by the rate of conversion of PAI-1 to latency when incubated at 37°C. The proportion of active PAI-1 was determined by its ability to inhibit trypsin, using a modification of the assay described by Gibson and Peterson [65]. PAI-1 at a final concentration of 6 μM in 50 mM Tris, pH 7.8, 15 mM NaCl, 0.1 mM EDTA, with or without an equimolar amount of vitronectin, was incubated at 37°C, with or without $MgCl_2$; the final concentration of Mg^{2+} was either 0.2 mM or 2 mM, relative to EDTA present. At various time points up to 3 h, an aliquot of the 6-μM PAI-1 was removed and diluted to 100 nM, in the same buffer except for a higher NaCl concentration (150 mM). Seventy microliters of this PAI-1 was mixed with an equal volume of 100 nM trypsin, prepared in 1 mM HCl. After a 5-min incubation at 37°C, residual trypsin activity was tested with addition of 60 μl of the PAI-1-trypsin mixture to 940 μl S-2222 chromogenic substrate (Chromogenix), having a final concentration of 100 μM, and also having been equilibrated to 37°C for 5 min. After 2 min at 37°C, the reaction was quenched by addition of 100 μl of 10% (w:v) SDS. The amount of substrate cleaved by trypsin was determined by reading the sample absorbance at 380 nm. The percent inhibition by PAI-1 was calculated relative to trypsin activity in the absence of

PAI-1. Percent inhibition was converted to PAI-1 activity, which was normalized to 100% activity for time = 0 min of incubation of 6 μM PAI-1 at 37°C.

Calculation of Standard Error

Standard error was calculated using the following equation:

$$\text{standard error} = \frac{1}{\sqrt{n}} \times \text{sample standard deviation}$$

where

$$\text{sample standard deviation} = \sqrt{\frac{\sum_{i=1}^{n} x_i^2 - n\left(\bar{x}\right)^2}{n-1}}$$

for n = number of data points; x_i = current data value; $\bar{x}$ = mean of data.

Results

Metal binding assessment by EPR

Both vitronectin and PAI-1 were tested for binding to two paramagnetic metals, Mn^{2+} and Cu^{2+}. A summary of the range of protein and metal concentrations tested is presented in Table 1. At room temperature, Mn^{2+} produces a useful EPR spectrum of six clearly defined peaks, even at low micromolar concentrations. The average of the six peak heights varies linearly with the concentration of free Mn^{2+} in the sample, for the range of concentrations used in these experiments. Therefore, this characteristic of the spectrum was used as a measure of free metal concentration in a sample. An example of an EPR

Table 1: Proteins and metals tested by EPR

Protein	Protein conc. range (μM)	Metal	Metal conc. range (μM)	Metal:Protein range	Binding indicated?
Vn	11-34	Mn^{2+}	5-50	0.25:1 to 4:1	No
PAI-1	11-30	Mn^{2+}	5-50	0.16:1 to 4.4:1	No
PAI-1-Vn	11-20	Mn^{2+}	5-50	0.25:1 to 4.4:1	No
PAI-1	25-50	Cu^{2+}	50-500	2:1 to 11.5:1	Yes

spectrum for 20 μM Mn^{2+} is shown in Figure 8. Experimental conditions and instrument parameters for spectroscopy with Mn^{2+} are readily available in the literature.

The spectrum for Cu^{2+} is less clearly defined, and most spectra in the literature were acquired with fairly high metal concentrations and at liquid nitrogen temperature (see *e.g.* [60] and [61]). Therefore, optimization of experimental conditions and instrument parameters was necessary before commencing room-temperature experiments on Cu^{2+} binding by our proteins.

Three main areas of experimental conditions required optimization before collecting EPR data for Cu^{2+} binding: conditions for using EPR to measure Cu^{2+} concentration in solution at room temperature; the validity of using this technique to demonstrate Cu^{2+} binding by protein; and solubility of PAI-1 in a non-Cu^{2+}-binding buffer and in the presence of Cu^{2+} itself.

By trial and error, instrument settings and Cu^{2+} concentrations were identified that produced a useful room-temperature EPR spectrum. Subtraction of a background spectrum obtained for the buffer in the absence of metal, resulted in a spectrum with a pattern like that depicted in Figure 9. Upon investigation of several features of the spectrum, one characteristic was identified to be most affected by Cu^{2+} concentration and also to vary linearly with concentration. The integral of the curve bounded by two certain points, indicated as *a* and *b* in Figure 9, was chosen as the characteristic to relate the measured spectrum to free Cu^{2+} concentration. The area under the curve is referred to as the peak intensity. A plot of intensity vs. concentration produced a standard curve like that shown in Figure 10.

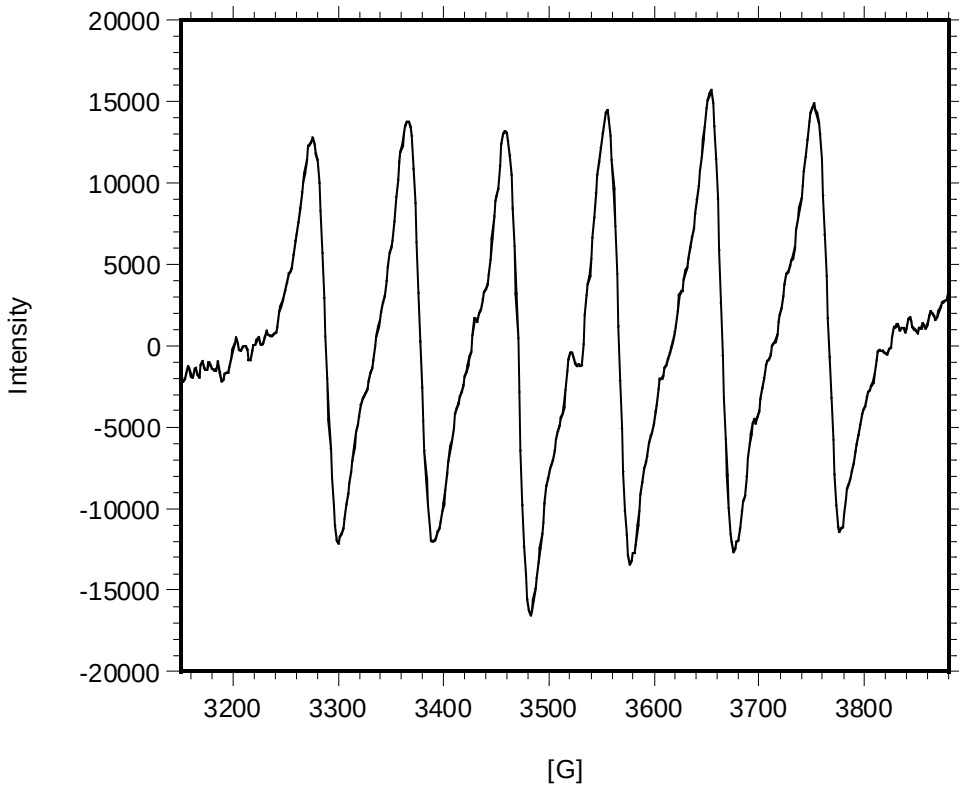


Figure 8: The EPR spectrum of Mn^{2+} has six distinct peaks.
An EPR spectrum of 20 μM Mn^{2+} in 25 mM Tris, pH 7.4, 0.15 M NaCl, was acquired at room temperature using microwave power of 6.82 mW and microwave frequency of 9.88 GHz. The average of the peak heights, which increase linearly with increasing concentration of free Mn^{2+}, were used as a measure of free Mn^{2+} concentration in a sample.

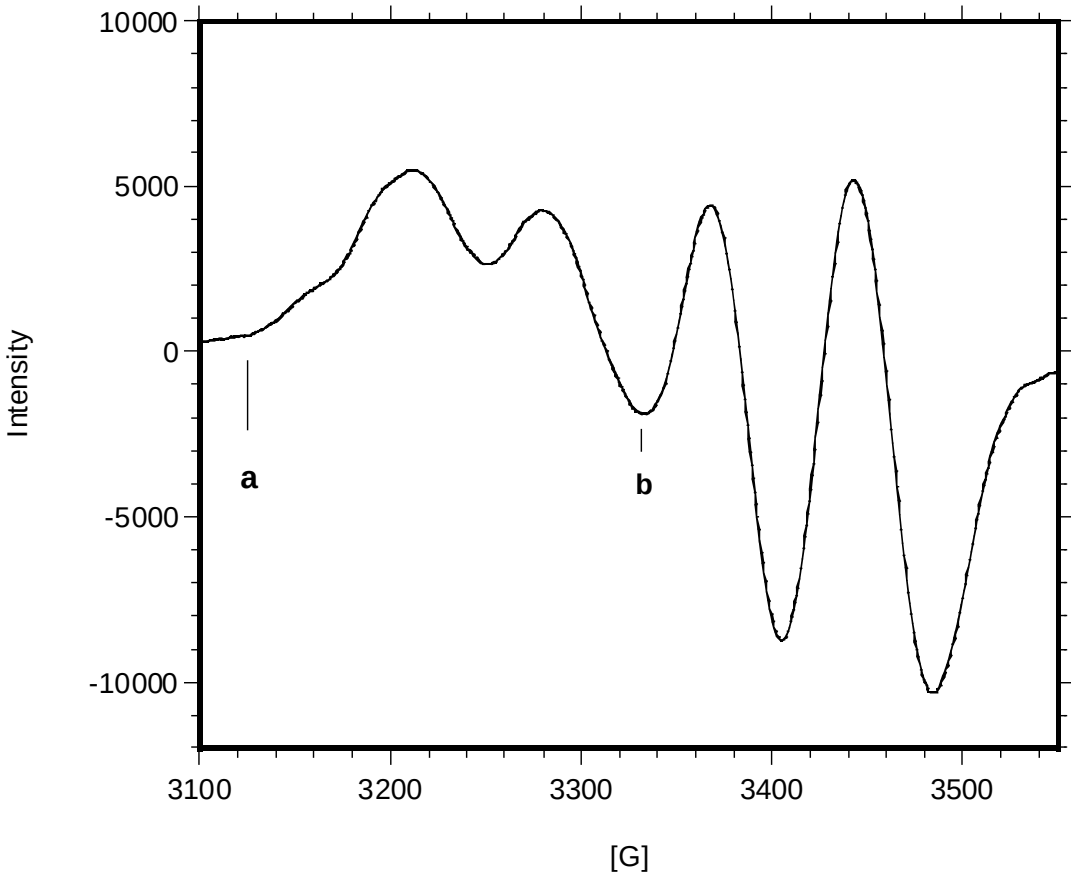


Figure 9: EPR spectrum for 200 μM Cu^{2+}.
An EPR spectrum of 200 μM Cu^{2+} in 10 mM ACES, pH 7.0, was acquired at room temperature using microwave power of 6.79 mW and microwave frequency of 9.88 GHz. The integral of the curve between *a* and *b* was found to increase linearly with free Cu^{2+} concentration, and was used as a measure of free Cu^{2+} in a sample. These conditions were used for BSA-Cu^{2+} studies.

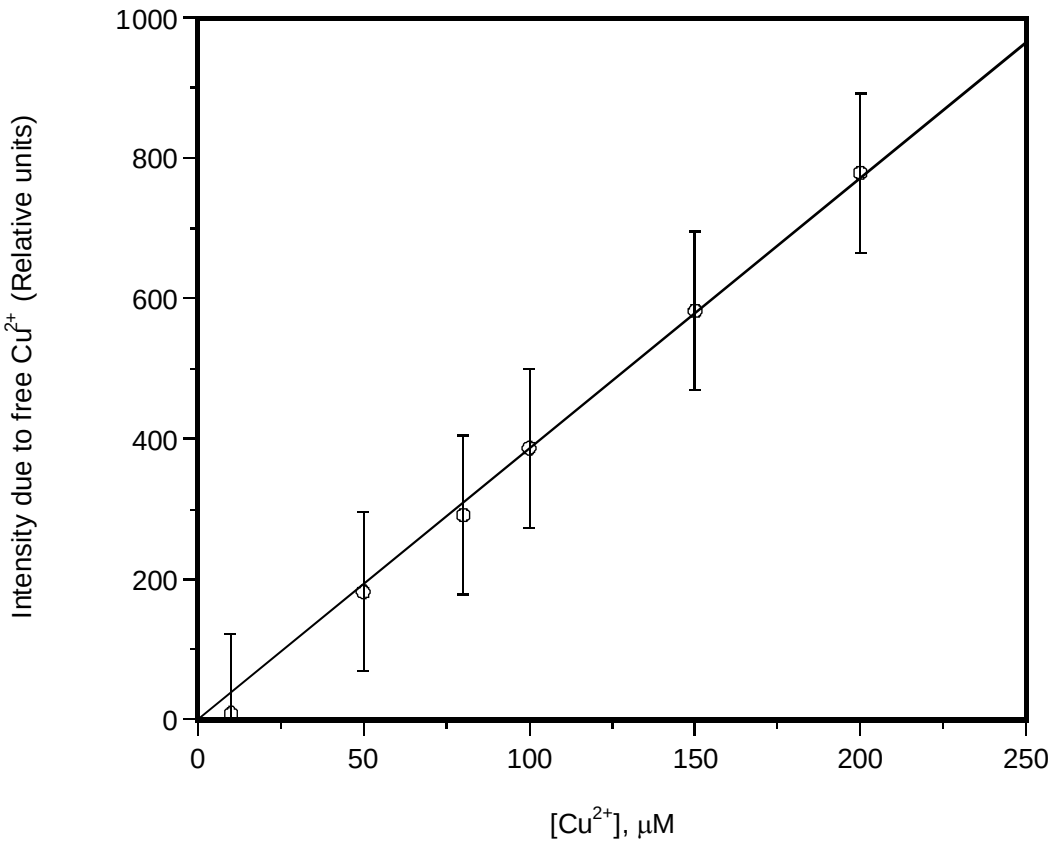


Figure 10: Standard curve for Cu^{2+} EPR peak intensity.
EPR spectra of Cu^{2+} in 10 mM ACES, pH 7.0, were acquired at room temperature. Peak intensity was plotted against the concentration of Cu^{2+} in each sample. Each data point represents a single sample. The *solid line* represents a linear fit of the data. *Error bars* represent standard error.

BSA was used as a test protein to show that this technique is useful to demonstrate Cu^{2+} binding by protein. BSA is known to have multiple metal-binding sites [62], [66]. Cu^{2+} binding by BSA was demonstrated by a lower intensity due to free Cu^{2+} for BSA-containing samples compared to Cu^{2+}-only samples, as can be seen in Figure 11, for a high concentration of BSA and metal:protein ratios of 1:1 to 8:1. These results validated this technique for the study of Cu^{2+} binding by our proteins.

The final obstacle to the use of this technique was lack of solubility of PAI-1 in a non-Cu^{2+}-binding buffer and in the presence of Cu^{2+} itself. Buffer is an important consideration when testing metal interactions with proteins, because some buffering components can interact with metal ions. This can change the availability of metals to interact with protein, and obscure measurement of the effect of metals on the protein. Phosphate, in particular, interacts strongly with metal ions; unfortunately, this is a preferred buffer when working with PAI-1. Therefore, another buffer had to be chosen for PAI-1-Cu^{2+} experiments.

Five buffers were tested for PAI-1 solubility: ACES, MES, MOPS, HEPES, and unbuffered 0.15 M NaCl. A sixth buffer, Tris, was known to be acceptable for PAI-1 preparation, but was questionable regarding its extent of interaction with Cu^{2+}. After testing Cu^{2+} in water (pH below 6) and Cu^{2+} in Tris (pH 7.4), clear differences in the EPR spectra confirmed that this buffer interacts too strongly with Cu^{2+} to be an option for use. ACES is a good choice for Cu^{2+} binding experiments, and was used for all BSA-Cu^{2+} testing. However, upon dialysis into ACES, PAI-1 visibly precipitated. Dialysis into MES and MOPS also resulted in precipitated PAI-1. PAI-1 was soluble in HEPES and in unbuffered 0.15 M NaCl, but upon addition of Cu^{2+} to either sample, the protein

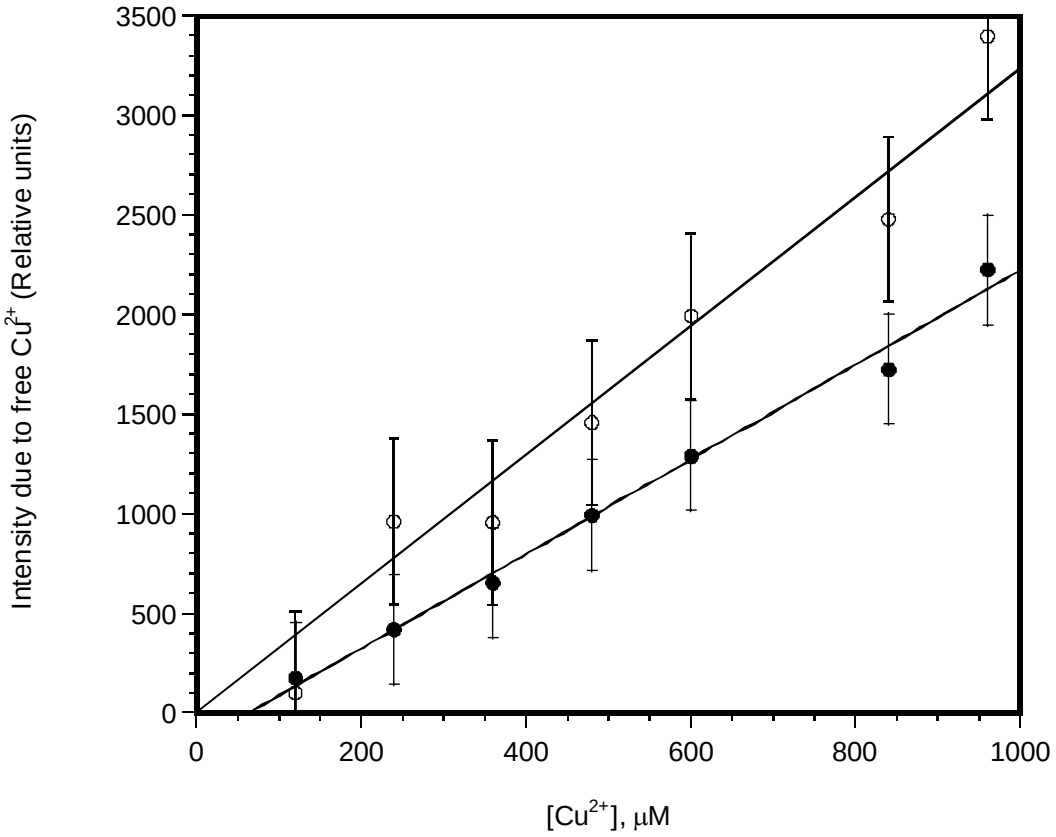


Figure 11: Test for Cu^{2+}-binding by BSA.
EPR spectra of Cu^{2+}, alone *(open circles),* or with 120 μM BSA *(closed circles),* in 10 mM ACES, pH 7.0, were acquired at room temperature. Peak intensity due to free Cu^{2+} was plotted against the total concentration of Cu^{2+} in each sample. Metal binding is indicated by the lower intensity of the metal + protein samples. Each data point represents the average intensity of two samples. The *solid lines* represent linear fits of the data. *Error bars* represent standard error.

precipitated, preventing collection of meaningful EPR data. Furthermore, while HEPES was believed not to interact strongly with Cu^{2+}, the use of this buffer in subsequent experiments with Cu^{2+} and vitronectin showed that it does interact with Cu^{2+}. This finding was confirmed by a recent report in the literature [67].

Various stabilizing agents added to Tris or HEPES also were tested for their potential to help maintain PAI-1 in a soluble form. However, polyethylene glycol (PEG) 8000 (0.1%), 360 mM sorbitol, and 1M NaCl were all unsuccessful in maintaining PAI-1 solubility.

Because unbuffered 0.15 M NaCl was the only solvent that both kept PAI-1 in solution until Cu^{2+} addition and did not interfere with metal-binding measurements, it was selected for further testing. Each PAI-1 sample, prepared in 0.15 M NaCl with a pH adjusted to 6 or lower, was mixed with Cu^{2+} and allowed to incubate at room temperature for 1 – 2 min., before centrifugation to pellet any precipitated sample, which was visible in some instances. Although insoluble material was not observed in most samples, each was centrifuged to maintain consistent treatment of samples. The supernatant was transferred to a new sample tube, and each supernatant tested by EPR. This method resulted in a repeatable decrease in free Cu^{2+} that varied with the amount of Cu^{2+} added to the protein. Therefore, this method was used to assess Cu^{2+} binding by PAI-1.

It should be noted that the Cu^{2+} spectrum used for the PAI-1 study is similar, but not identical, to that used for the BSA study, as previously shown in Figure 9. The difference is due to adjustments made to the instrument settings and data acquisition parameters, which permitted more straightforward data analysis. As can be seen from the example spectrum presented in Figure 12, the EPR spectrum for Cu^{2+} that was used for the PAI-1

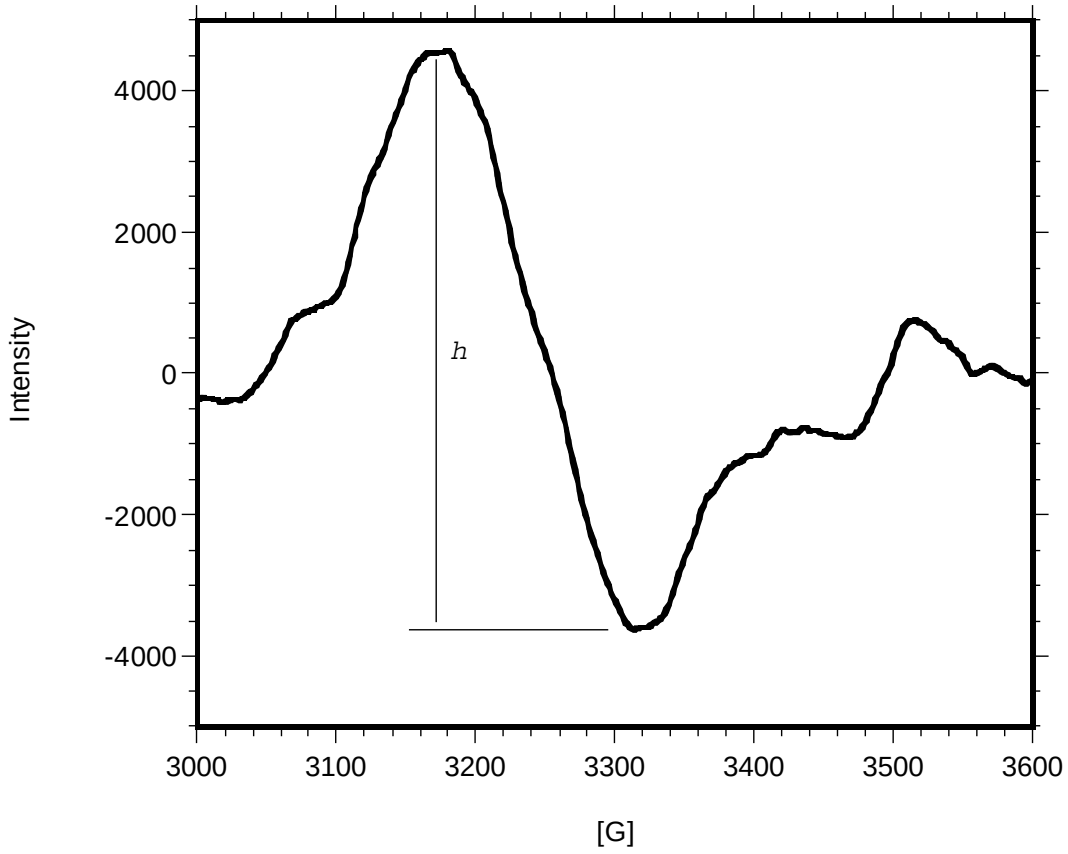


Figure 12: EPR spectrum for 150 μM Cu^{2+} showing the height (h) used as a measure of concentration.

An EPR spectrum of 150 μM Cu^{2+} in unbuffered 0.15 M NaCl with a pH below 6.0, was acquired at room temperature using microwave power of 21.6 mW and microwave frequency of 9.88 GHz. The peak height, *h,* was found to increase linearly with free Cu^{2+} concentration, and was used as a measure of free Cu^{2+} in a sample. These conditions were used for PAI-1-Cu^{2+} studies.

study has several peaks, one of which is considerably larger than the others. The peak-to-trough height was found to increase linearly with the concentration of free metal in the sample, for the range of concentrations used in these experiments. Therefore, this characteristic of the spectrum was used as a measure of free metal concentration in a sample. A comparison of several spectra illustrating the increase in peak height with increasing concentration is presented in Figure 13.

As shown by the differing heights of the EPR spectra depicted in Figures 14 and 15, PAI-1 binds Cu^{2+}. The data set for a range of Cu^{2+} concentrations is plotted in Figure 16. Scatchard analysis of the binding data allows calculation of an approximate Kd equal to or below 15 μM, and a stoichiometry of at least 5:1 metal:protein (Figure 17). However, this method is not sensitive enough for complete characterization of the binding interaction (*i.e.*, definitive determination of affinity and total number of binding sites, for both the tighter and the weaker interactions); for Cu^{2+} concentrations below 100 μM, the signal is not clearly distinguishable from the noise. Data from samples containing less than 100 μM Cu^{2+} would be needed for complete characterization of this binding interaction.

Vitronectin was shown not to bind Mn^{2+}, when tested over a metal:protein range from 0.25:1 to 1:1 (see Figure 18). Substoichiometric metal concentrations were used because this condition is necessary to detect weak binding. Other experiments, using as high as a 4:1 metal:protein ratio, also failed to indicate Mn^{2+} binding by vitronectin (data not shown). Similarly, PAI-1 and the complex of PAI-1-vitronectin were shown not to bind Mn^{2+} (see Figures 19 and 20). Higher metal concentrations also failed to indicate binding (data not shown).

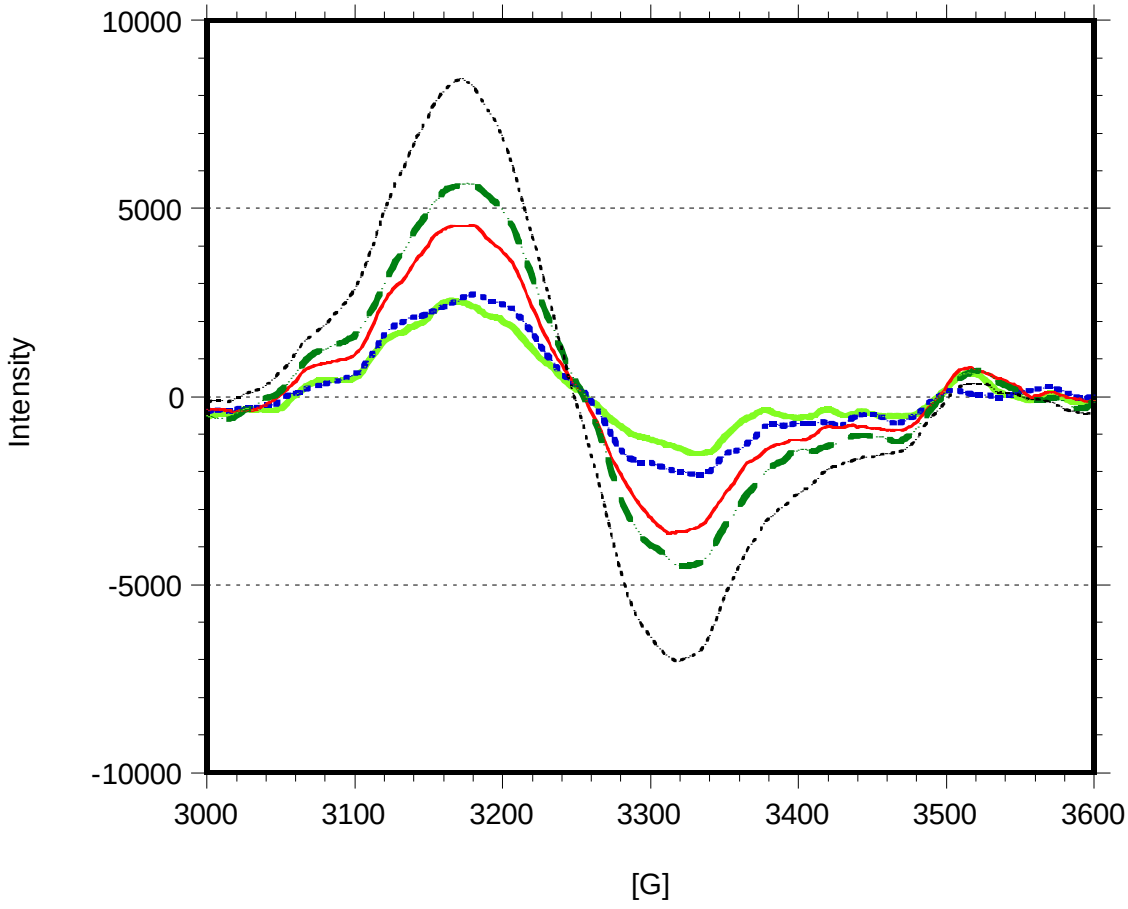


Figure 13: Overlaid EPR spectra for 75 to 300 μM Cu^{2+}.
EPR spectra of Cu^{2+} in unbuffered 0.15 M NaCl with a pH below 6.0, were acquired at room temperature using microwave power of 21.6 mW and microwave frequency of 9.88 GHz. Cu^{2+} concentrations represented are: 75 μM *(thick, solid line)*; 100 μM *(thick, dotted line)*; 150 μM *(thin, solid line)*; 200 μM *(thick, dashed line)*; and 300 μM (*thin, dotted line*).

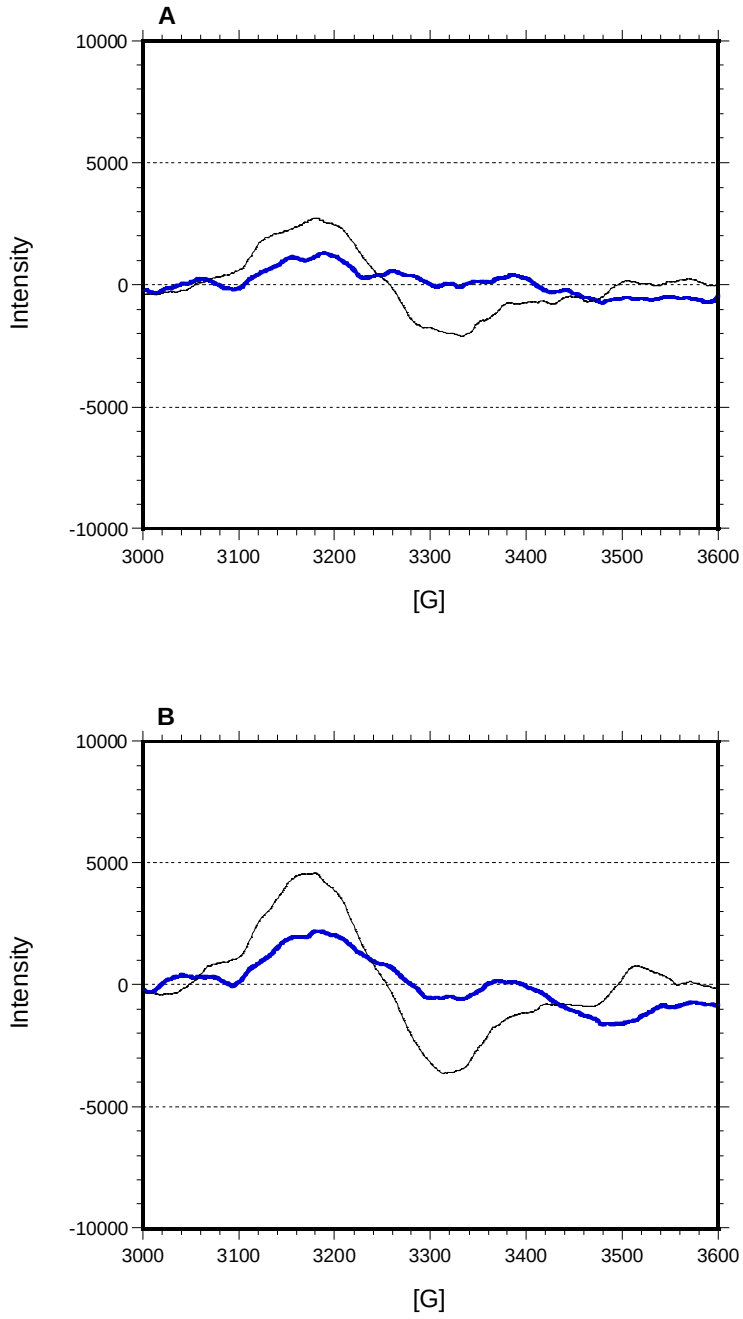


Figure 14: EPR spectra for (*A*) 100 μM and (*B*) 150 μM Cu^{2+}, with and without 25 μM PAI-1.

EPR spectra of Cu^{2+} alone (*thin line*) or with 25 μM PAI-1 (*thick line*) in unbuffered 0.15 M NaCl with a pH below 6.0, were acquired at room temperature using microwave power of 21.6 mW and microwave frequency of 9.88 GHz. Binding is indicated by the lower intensity of the metal + protein sample.

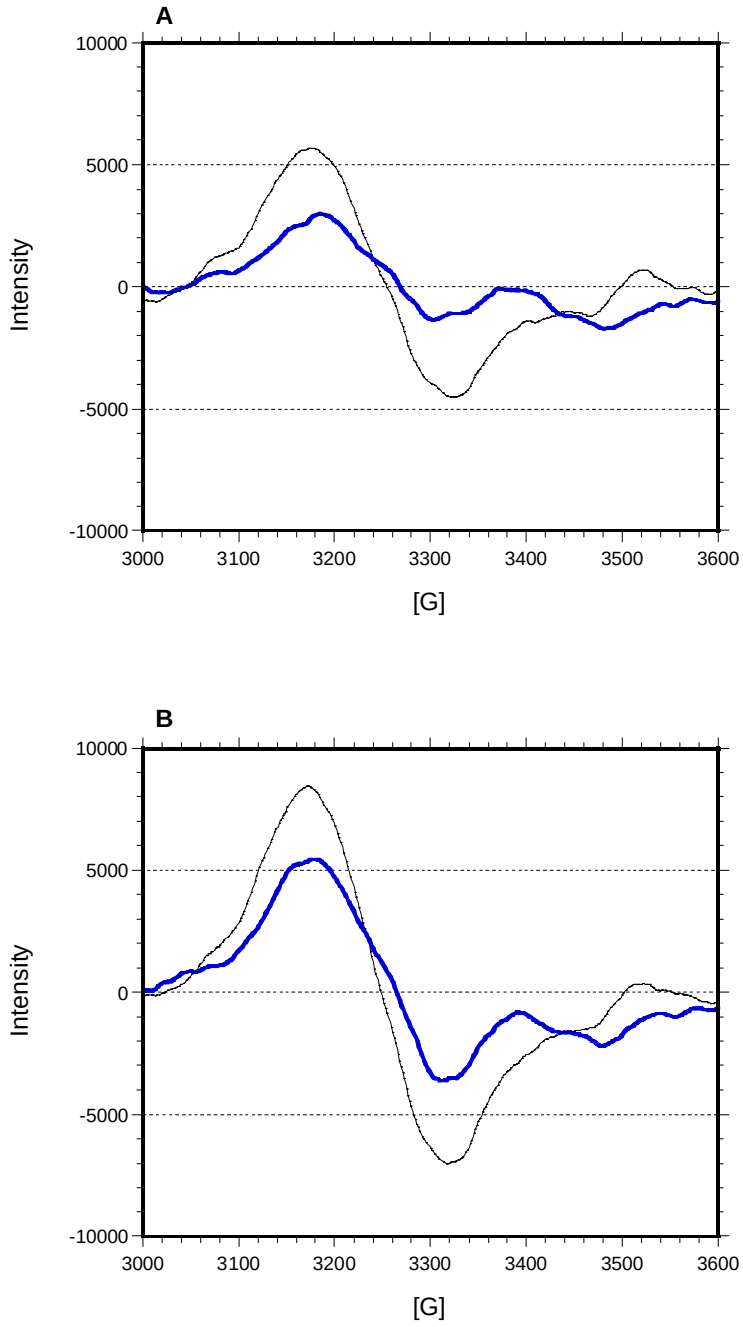


Figure 15: EPR spectra for (*A*) 200 μM and (*B*) 300 μM Cu^{2+}, with and without 25 μM PAI-1.

EPR spectra of Cu^{2+} alone (*thin line*) or with 25 μM PAI-1 (*thick line*) in unbuffered 0.15 M NaCl with a pH below 6.0, were acquired at room temperature using microwave power of 21.6 mW and microwave frequency of 9.88 GHz. Binding is indicated by the lower intensity of the metal + protein sample.

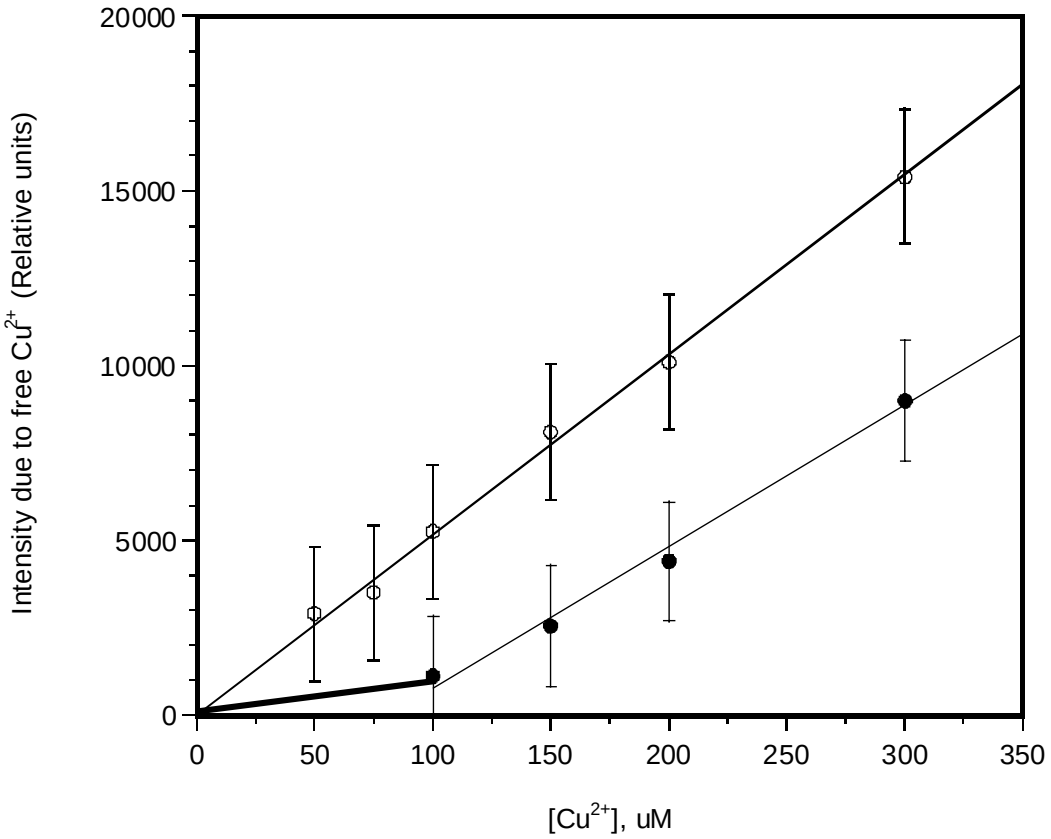


Figure 16: Test for Cu^{2+}-binding by 25 μM PAI-1.
EPR spectra of Cu^{2+} alone *(open circles)* or with 25 μM PAI-1 *(closed circles),* in unbuffered 0.15 M NaCl with a pH below 6.0, were acquired at room temperature. Peak intensity due to free Cu^{2+} was plotted against the total concentration of Cu^{2+} in each sample. Metal binding is indicated by the lower intensity of the metal + protein samples. Each data point represents the average intensity of two samples. The *thin lines* represent linear fits of the data, while the *thick line* estimates the tighter binding of the suspected class of higher-affinity Cu^{2+}-binding sites. *Error bars* represent standard error.

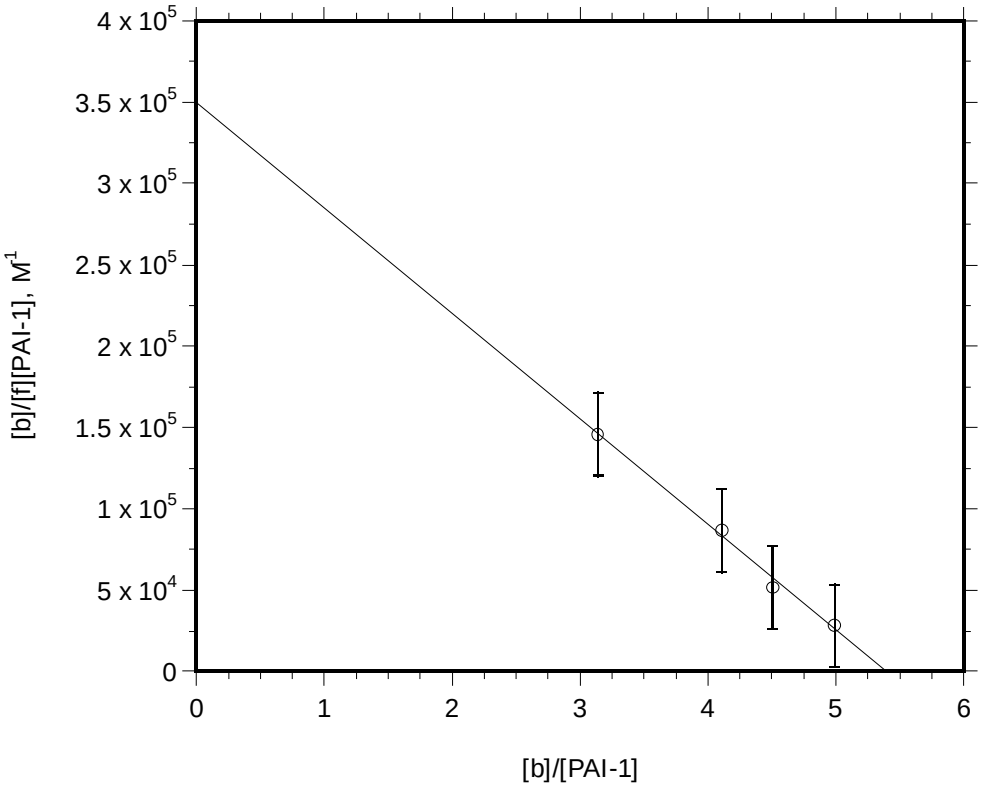


Figure 17: Scatchard plot for Cu^{2+}-binding by 25 μM PAI-1.
[b] and *[f]* represent concentration of bound Cu^{2+} and free Cu^{2+}, respectively. *Line* represents linear fit of data. The negative slope of the fit line, 15 μM, is an estimate of the Kd for PAI-1- Cu^{2+}. The *x-intercept*, 5.4, is an estimate of the number of binding sites for Cu^{2+} on PAI-1. *Error bars* represent standard error.

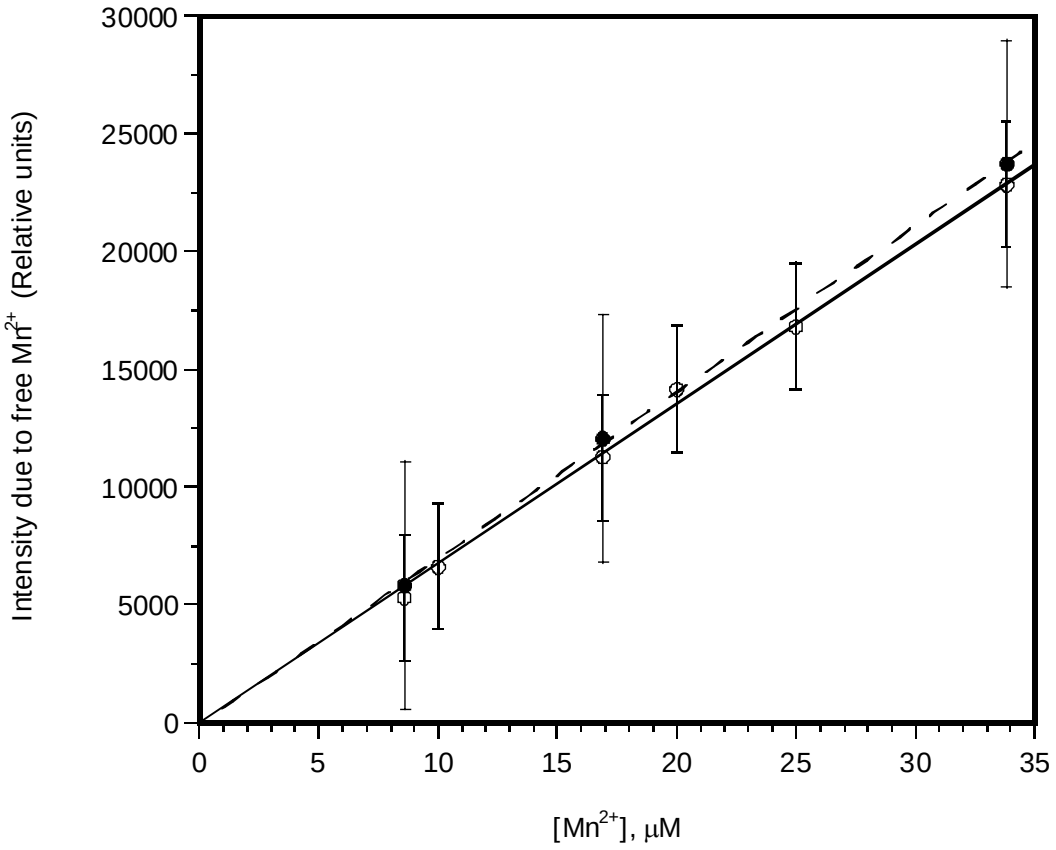


Figure 18: Test for Mn^{2+}-binding by 34 μM Vn.
EPR spectra of Mn^{2+} alone *(open circles)* or with 34 μM Vn *(closed circles),* in 25 mM Tris, pH 7.4, 0.15 M NaCl, were acquired at room temperature. Peak intensity due to free Mn^{2+} was plotted against the total concentration of Mn^{2+} in each sample. The intensity due to free Mn^{2+} does not decrease in the presence of protein, indicating no metal bound by the protein. Each data point represents the average intensity of two samples. *Lines* represent linear fits of the data for Mn^{2+} alone (*solid)* or Mn^{2+} + Vn (*dashed)*. *Error bars* represent standard error.

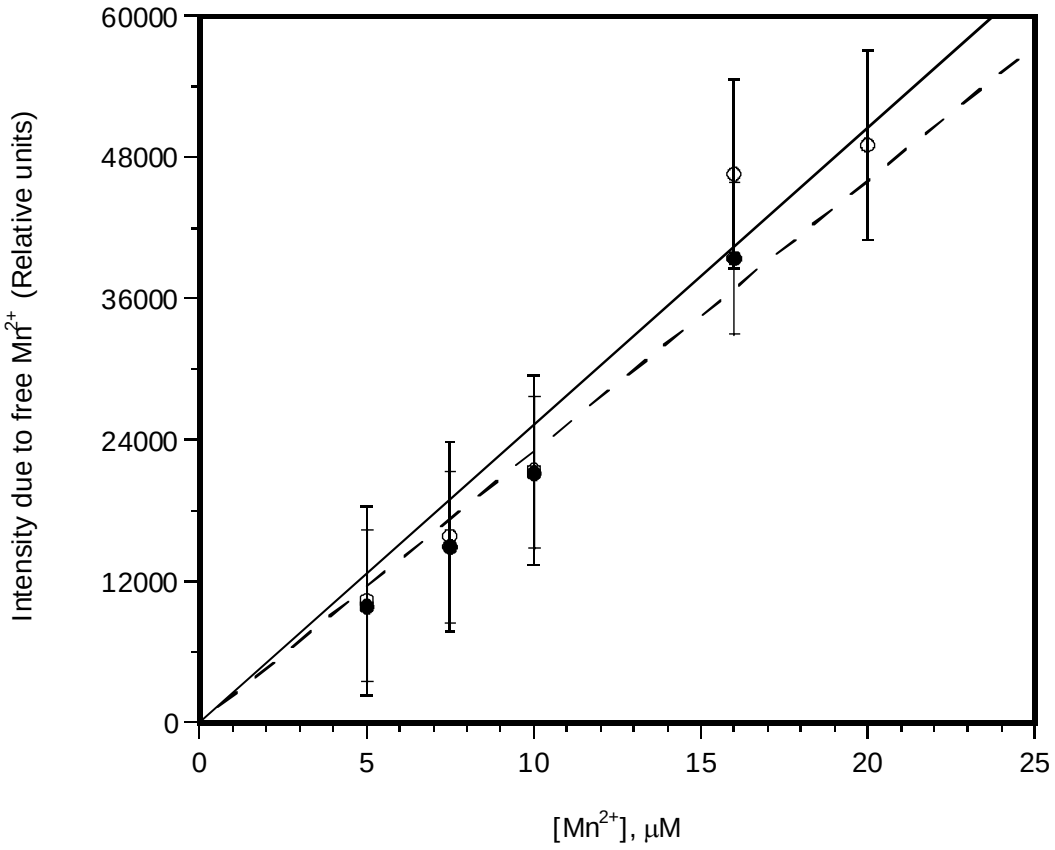


Figure 19: Test for Mn^{2+}-binding by 30 μM PAI-1.
EPR spectra of Mn^{2+} alone *(open circles)* or with 30 μM PAI-1 *(closed circles)*, in 25 mM Tris, pH 7.4, 0.15 M NaCl, were acquired at room temperature. Peak intensity due to free Mn^{2+} was plotted against the total concentration of Mn^{2+} in each sample. The intensity due to free Mn^{2+} does not decrease in the presence of protein, indicating no metal bound by the protein. Each data point represents the average intensity of two samples. *Lines* represent linear fits of the data for Mn^{2+} alone (*solid)* or Mn^{2+} + PAI-1 (*dashed)*. *Error bars* represent standard error.

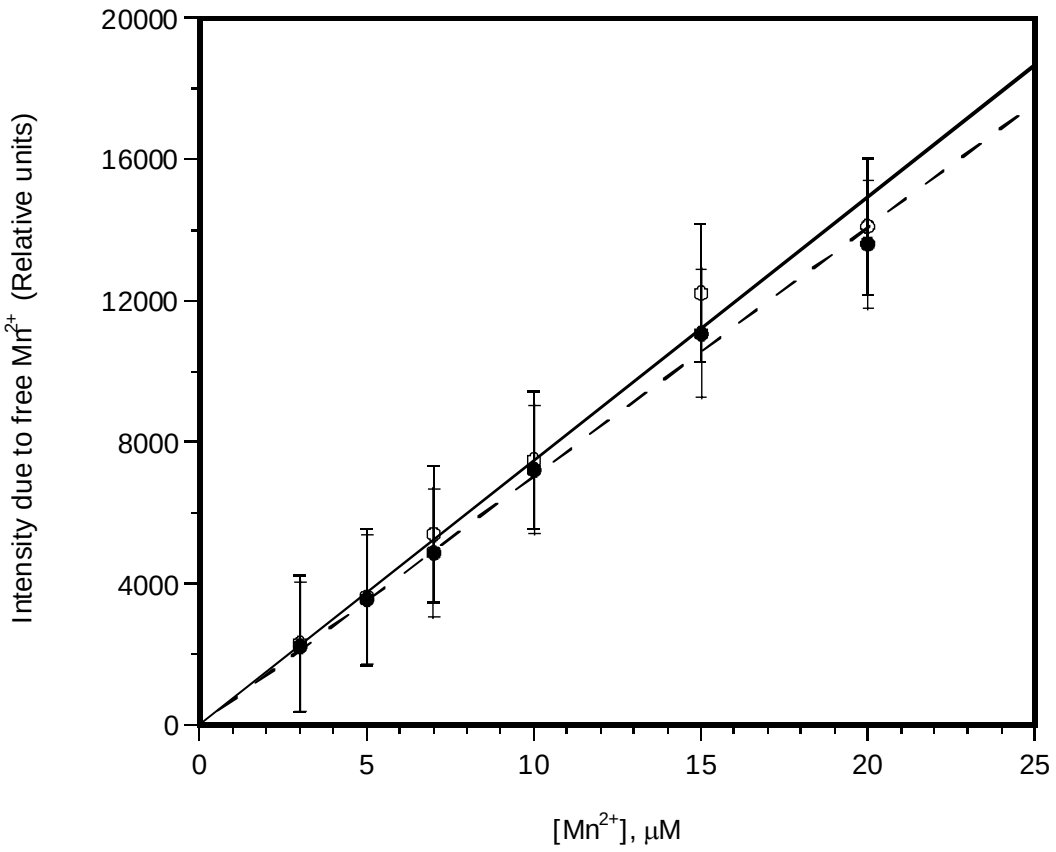


Figure 20: Test for Mn^{2+}-binding by 20 μM PAI-1-Vn.
EPR spectra of Mn^{2+} alone *(open circles)* or with 20 μM PAI-1-Vn *(closed circles),* in 25 mM Tris, pH 7.4, 0.15 M NaCl, were acquired at room temperature. Peak intensity due to free Mn^{2+} was plotted against the total concentration of Mn^{2+} in each sample. The intensity due to free Mn^{2+} does not decrease in the presence of protein, indicating no metal bound by the protein. Each data point represents the average intensity of two samples. *Lines* represent linear fits of the data for Mn^{2+} alone *(solid)* or Mn^{2+} + PAI-1-Vn *(dashed)*. *Error bars* represent standard error.

Mg^{2+} has no measurable effect on PAI-1 activity or on stabilization by vitronectin

A diagram presenting the procedure for the kinetic assay used to assess PAI-1 activity is shown in Figure 21. Kinetic testing revealed that, under the conditions of the assay, Mg^{2+} has no measurable effect on PAI-1 activity or on PAI-1 stabilization by vitronectin. PAI-1 exhibited the same amount of inhibitory activity towards trypsin, and lost this activity at a similar rate, in the presence and absence of Mg^{2+}. Furthermore, vitronectin stabilized PAI-1 for the same length of time in the presence and absence of Mg^{2+}. Attempts to test the effect of Ca^{2+} failed due to technical difficulties, including intermittent precipitation of the sample upon incubation with Ca^{2+}, and poor repeatability of results.

Considerable optimization of experimental conditions was necessary before using this assay to determine the effect of Mg^{2+} on our proteins. The initial step towards optimizing the assay was determining appropriate concentrations of substrate and trypsin to use, to give adequate end absorbance with room for detecting a decrease upon PAI-1 inhibition. Early problems were two-fold: poor repeatability, despite careful control of conditions; and low final absorbance, despite testing a range of substrate concentrations, including concentrations much higher than recommended by the manufacturer.

The low final absorbance was traced to the trypsin supply. The original choice for the enzyme was Promega sequencing-grade trypsin; however, although a higher grade, Promega trypsin is not as active against the S-2222 substrate as is Sigma trypsin. An additional modest increase in absorbance was realized by determining that the actual peak wavelength of absorbance is 380 nm, instead of the reported 405 nm for the released pNA

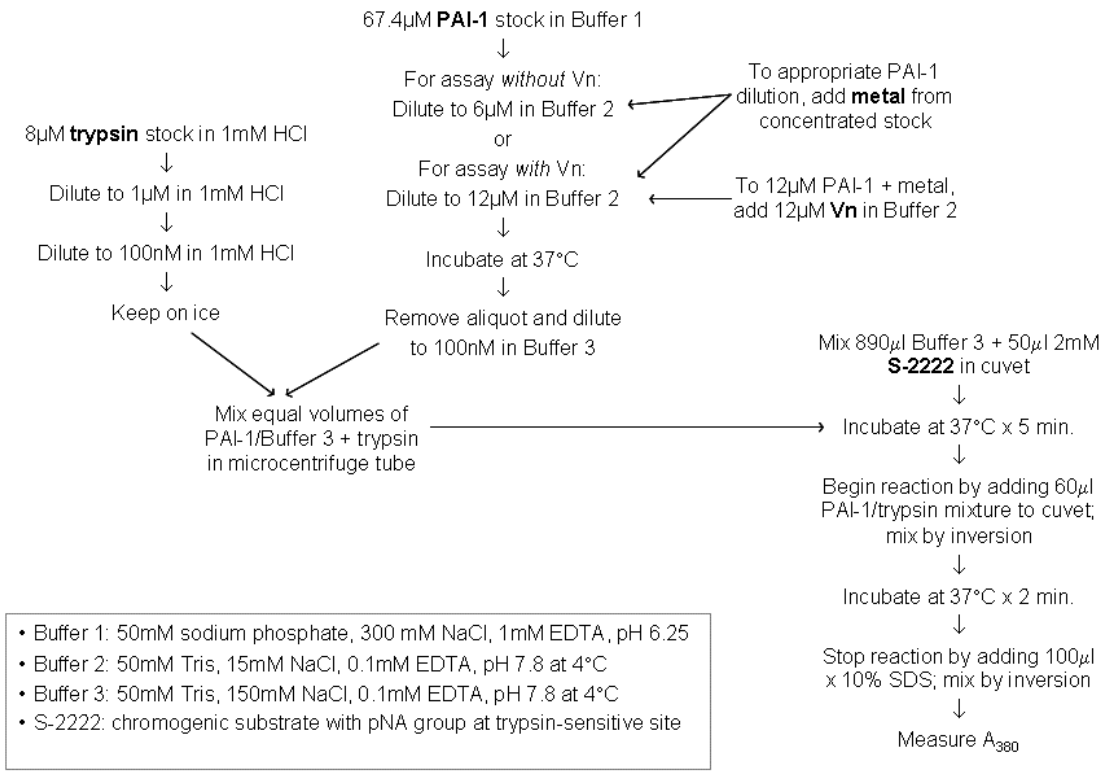


Figure 21: Kinetic assay to test PAI-1 activity.

group. Changing the trypsin source and the wavelength for absorbance measurement resulted in a higher final absorbance from the assay, allowing maximum opportunity for detecting a decrease in absorbance upon addition of PAI-1 to the assay.

The poor repeatability was traced to self-degradation of substrate in the solution conditions recommended by the manufacturer (lyophilized stock dissolved in water or buffer, stored at 4°C). Even in the absence of trypsin, a slow increase in absorbance could be measured for a solution of substrate in real time. A substrate solution made in 1mM HCl was found to be stable; aliquots frozen at -20°C permitted long-term storage of substrate stock in 1mM HCl.

We needed to identify conditions such that PAI-1 was even less stable than under physiological conditions. This would permit monitoring PAI-1 activity, when stabilized by vitronectin, over an increased time span. A low-salt buffer containing 15 mM NaCl in Tris, instead of physiological, 150 mM NaCl, was used for PAI-1 at a concentration of 6 μM. These conditions resulted in PAI-1 being stable at 4°C for a suitably long time, while losing activity rapidly at 37°C. It should be noted that PAI-1 was diluted into Tris with 150 mM salt before incubation with trypsin, and the actual cleavage reaction of the assay was also performed in Tris with 150 mM salt.

Initial experiments were performed with the reaction occurring in a temperature-controlled cell, which allowed monitoring of the rate of reaction at 37°C. This method was used to confirm the linear range of the reaction. Determination of the time-frame of linearity allowed using an end-point measurement of absorbance, quenching the reaction at a given time within the linear range of the reaction, and then reading the absorbance.

This allowed duplicate reactions to be run simultaneously. Several reagents were tested to find a suitable one that stopped the reaction without diluting the sample excessively, changing the final absorbance excessively, or shifting the peak wavelength. Reagents that were tested include NaOH, HCl, and SDS. A two-minute end point was chosen, and the reaction was quenched by addition of 100 μl of SDS (10%, w:v).

The results of the kinetic assays are shown graphically in Figures 22, 23, and 24. Comparison of the data sets in Figure 22 shows that the rate of loss of PAI-1 inhibitory activity is the same in the presence and in the absence of Mg^{2+}. Likewise, as comparison of the data sets in Figure 23 shows, the ability of vitronectin to stabilize PAI-1 is the same in the presence and in the absence of Mg^{2+}. A comparison of the stability of PAI-1 in the presence and absence of vitronectin, confirming the characteristic stabilizing effect of vitronectin towards PAI-1, is shown in Figure 24. Analysis of these results together demonstrates that, under the conditions of this assay, Mg^{2+} has no measurable effect on PAI-1 activity or on PAI-1 stabilization by vitronectin.

Discussion and Future Directions

Metal-binding studies

We have shown that EPR is not an effective method for quantifying metal binding by PAI-1 and vitronectin, although it is somewhat effective for qualifying binding, *i.e.*, determining whether binding exists. As a means of studying the solution interaction between PAI-1 and metals, it is a good complementary technique to the IMAC studies described earlier.

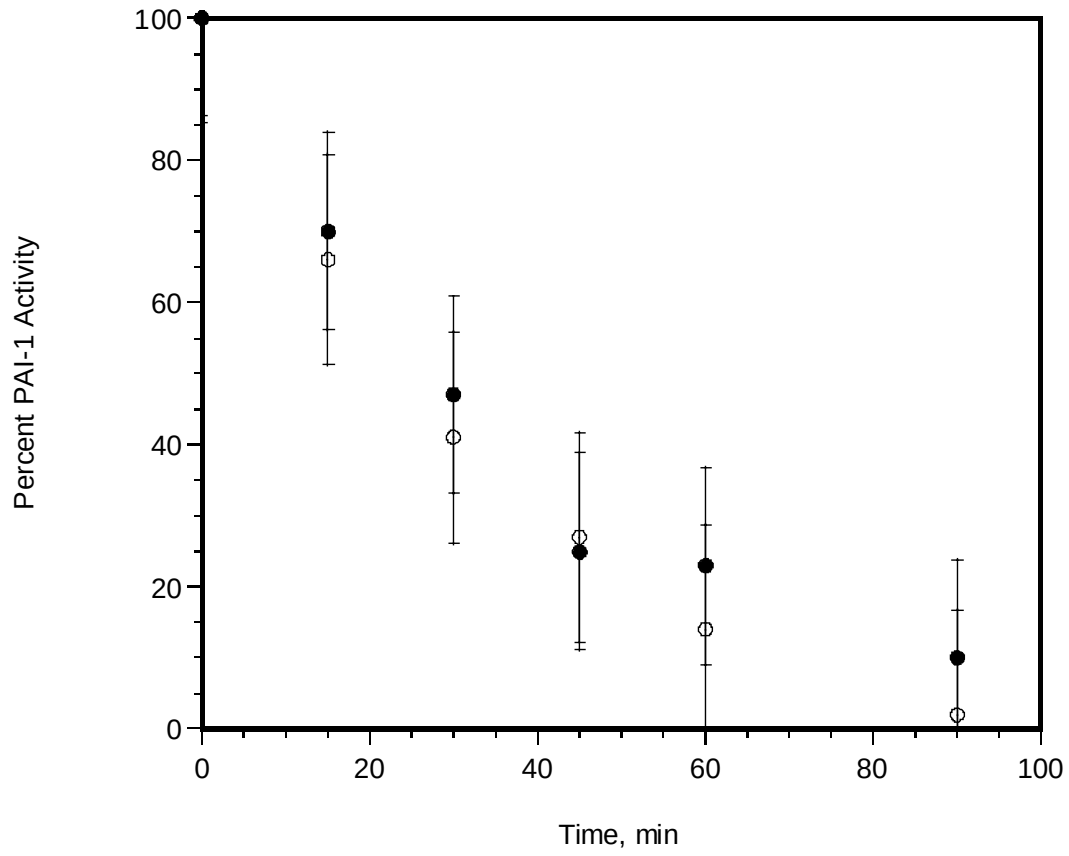


Figure 22: Kinetic assay to measure activity of PAI-1 +/- Mg^{2+}.
PAI-1 at a final concentration of 6 μM in 50 mM Tris, pH 7.8, 15 mM NaCl, 0.1 mM EDTA, was incubated at 37°C, either alone *(open circles)* or with 2 mM $MgCl_2$ (relative to EDTA; *closed circles*). At various time points, an aliquot of PAI-1 was diluted to 100 nM, in the same buffer except for a higher NaCl concentration (150 mM), and mixed with an equimolar amount of trypsin. After a 5-min incubation at 37°C, residual trypsin activity was measured using S-2222 chromogenic substrate, as described in *Materials and Methods*. Percent inhibition of trypsin by PAI-1 was calculated relative to trypsin activity in the absence of PAI-1. Percent inhibition was converted to PAI-1 activity, which was normalized to 100% activity for time = 0 min of incubation of 6 μM PAI-1 at 37°C. Each data point represents the average of two samples. *Error bars* represent standard error.

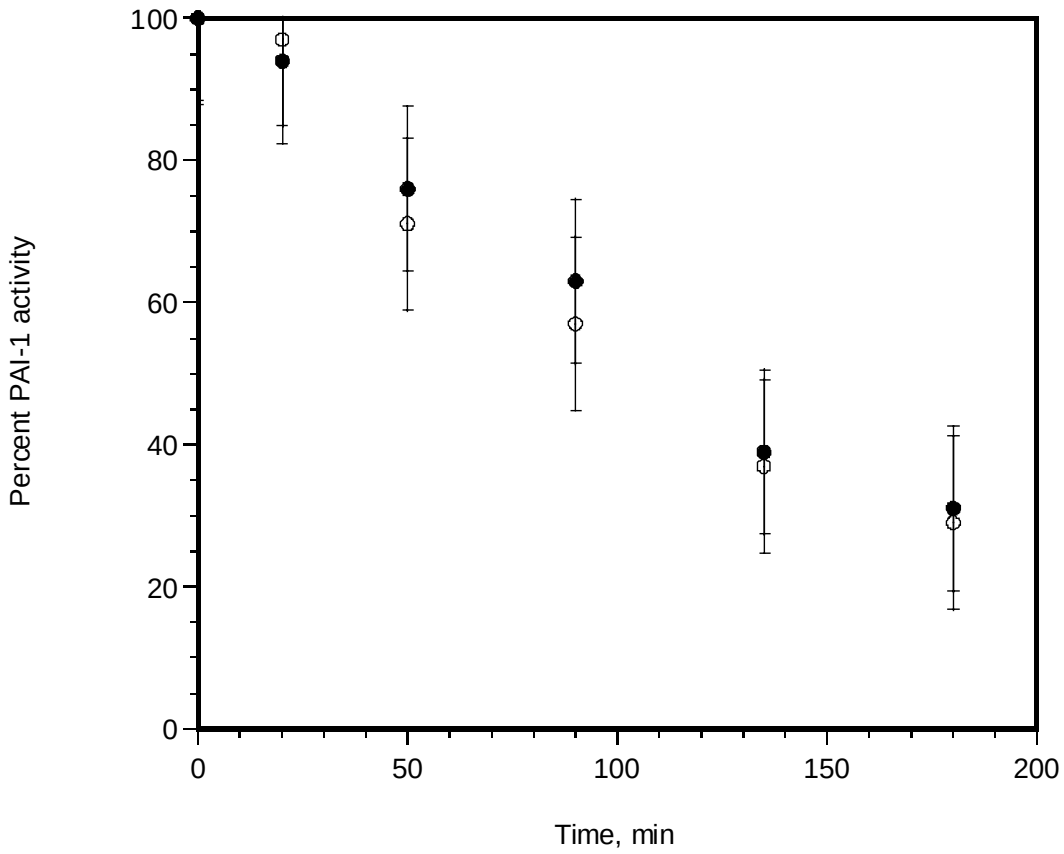


Figure 23: Kinetic assay to measure activity of PAI-1-Vn +/- Mg^{2+}.
Equimolar PAI-1-Vn complex at a final concentration of 6 μM in 50 mM Tris, pH 7.8, 15 mM NaCl, 0.1 mM EDTA, was incubated at 37°C, either alone *(open circles)* or with 2 mM $MgCl_2$ (relative to EDTA; *closed circles*). At various time points, an aliquot of PAI-1-Vn was diluted to 100 nM, in the same buffer except for a higher NaCl concentration (150 mM), and mixed with an equimolar amount of trypsin. After a 5-min incubation at 37°C, residual trypsin activity was measured using S-2222 chromogenic substrate, as described in *Materials and Methods*. Percent inhibition of trypsin by PAI-1 was calculated relative to trypsin activity in the absence of PAI-1. Percent inhibition was converted to PAI-1 activity, which was normalized to 100% activity for time = 0 min of incubation of 6 μM PAI-1-Vn at 37°C. Each data point represents the average of two samples. *Error bars* represent standard error.

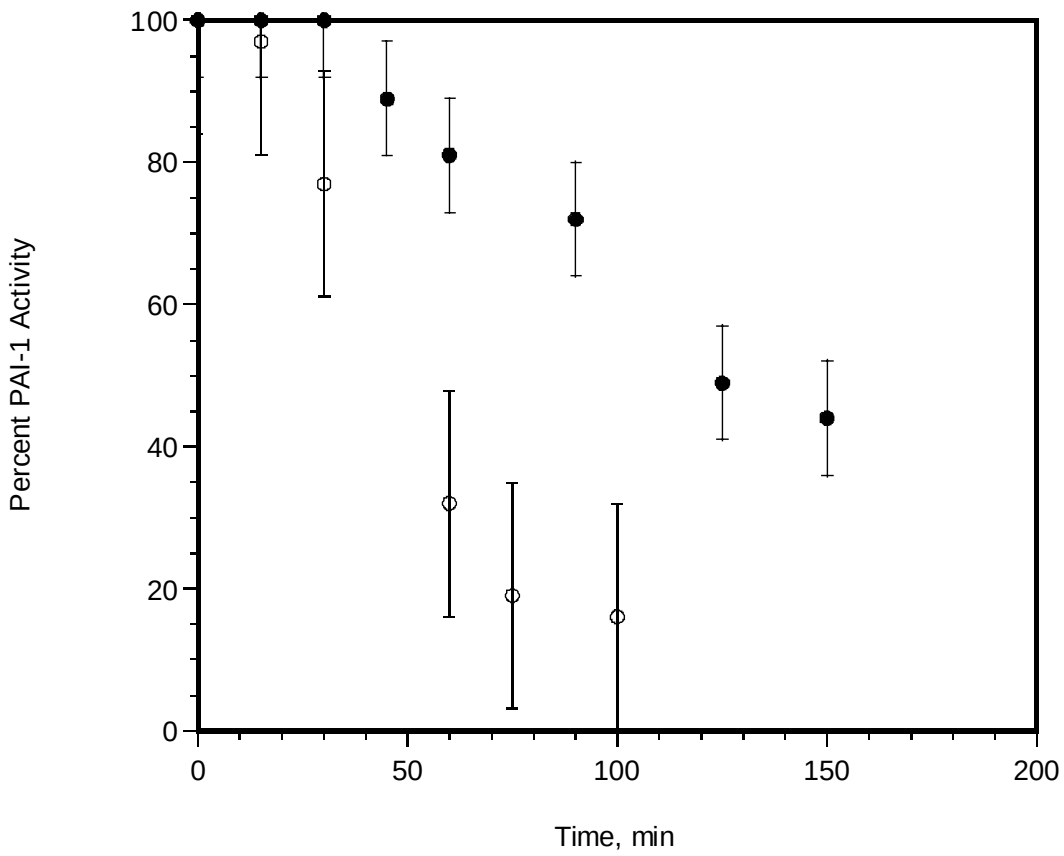


Figure 24: Kinetic assay to measure activity of PAI-1 +/- Vn.
PAI-1 alone *(open circles),* or equimolar PAI-1-Vn complex *(closed circles)*, at a final concentration of 6 μM in 50 mM Tris, pH 7.8, 15 mM NaCl, 0.1 mM EDTA, was incubated at 37°C. At various time points, an aliquot of PAI-1 or PAI-1-Vn was diluted to 100 nM, in the same buffer except for a higher NaCl concentration (150 mM), and mixed with an equimolar amount of trypsin. After a 5-min incubation at 37°C, residual trypsin activity was measured using S-2222 chromogenic substrate, as described in *Materials and Methods*. Percent inhibition of trypsin by PAI-1 was calculated relative to trypsin activity in the absence of PAI-1. Percent inhibition was converted to PAI-1 activity, which was normalized to 100% activity for time = 0 min of incubation of 6 μM PAI-1 or PAI-1-Vn at 37°C. Each data point represents the average of two samples. *Error bars* represent standard error.

It was found that PAI-1-Cu^{2+} binding is clearly detectable by EPR, but the method is not sensitive enough for determination of affinity and the number of binding sites; for Cu^{2+} concentrations below 100 μM, the signal is not clearly distinguishable from the noise. However, Scatchard analysis was performed for data from samples having at least 100 μM Cu^{2+}, allowing estimation of a maximum Kd equal to 15 μM, which indicates a reasonably tight affinity for at least one set of metal-binding sites on PAI-1. Scatchard analysis also allowed estimation of at least five sites having this maximum Kd. It is suspected that one or two sites with a lower Kd also exist, but this method is not amenable to characterization of such sites.

Another difficulty encountered in the study of Cu^{2+} binding is that buffer choices for Cu^{2+} measurements are few, because many standard buffers used with both of our proteins bind Cu^{2+} themselves. For this reason, PAI-1 experiments were done in water without buffer, with only NaCl. One vitronectin-Cu^{2+} experiment was performed, but its strange results led to further testing of potential Cu^{2+} binding by the buffer used (HEPES), revealing that the buffer did bind the metal in the experiment, such that Cu^{2+} binding by vitronectin could not be assessed. It could be worthwhile to try additional vitronectin-Cu^{2+} EPR experiments if a suitable buffer can be found, testing the 0.15 M NaCl solution as a first option. Even if quantitative conclusions are not possible, qualitative conclusions may be attainable.

Lack of binding detection between vitronectin or PAI-1 and the second paramagnetic metal tested, Mn^{2+}, may be due to such a weak affinity that it is too low to be measured by this method. Detection of weak affinity requires substoichiometric M:P samples, but

for such samples to be useful, either the metal must have a detectable EPR spectrum at low concentrations, or the protein must be stable at high concentrations. The tendency of our two proteins to aggregate at even moderate concentrations limits the highest concentration of protein possible for samples. Combined with the lower limit on detectable Mn^{2+}, these restrictions greatly narrow the range of M:P ratios that may be measured. Although Mn^{2+} has a useful EPR spectrum at low micromolar concentrations (below 10 μM), these concentrations are not very low in terms of our proteins. Only a narrow range of substoichiometric M:P samples are available for testing.

Based on our knowledge of specific but weak binding of PAI-1 to immobilized Mn^{2+}, the lack of binding detection between $Mn^{2+}$and PAI-1 in solution was not entirely unexpected. The "effective concentration" of an immobilized ligand is greater than the actual concentration of the same amount of ligand in solution. This is due to the higher likelihood that the binding molecule will encounter an immobilized ligand compared to a ligand in solution. Therefore, although Mn^{2+} binding by PAI-1 is indicated by the IMAC method, but is not indicated by EPR, these results are not contradictory.

For future work, an alternative technique to use for metal-binding studies is NMR. For both PAI-1 and the SMB domain, spectra could be acquired in the presence and in the absence of metals. Any peak shifts or other changes in the spectra would indicate metal binding. For the SMB domain, the existence of a solved NMR structure for this peptide [6] would aid in identifying peak shifts or other changes resulting from metal ions binding. A limitation of this method is that full-length vitronectin, at 62 kDa, is too large for NMR studies. However, an advantage of this method is that metal choices are not limited to those that are paramagnetic, as was a requirement for EPR experiments. Other

metals shown to bind PAI-1 by IMAC, including Co^{2+} (which is paramagnetic, but requires liquid nitrogen temperature for EPR study), Ni^{2+}, and Zn^{2+}, would be good candidates for metal-binding studies by NMR.

Absence of Mg^{2+} effect on PAI-1 activity and on stabilization by vitronectin

A kinetic assay was used to study the effect of metals on PAI-1 activity and stabilization by vitronectin. Although clearly showing no detectable effect of Mg^{2+}, these results are limited in two ways: they reflect only a single method of testing, and only a single metal was tested for its effect. Both Mg^{2+} and Ca^{2+} were initially chosen for investigation due to their presence and influence in our integrin-binding buffer. Because it is vitronectin which binds directly to integrins in the form of the vitronectin-PAI-1 complex, it was expected that these metals might have an effect, through binding to vitronectin, on stabilization of PAI-1. However, Mg^{2+} was shown to have no effect, and difficulty maintaining Ca^{2+} in solution when mixed with the PAI-1 sample prevented testing of the effect of this metal in the kinetic assay. It could be worthwhile to attempt further optimization of conditions that permit assaying the effect of Ca^{2+} on PAI-1 activity or stabilization by vitronectin. In addition, based on the results of PAI-1 binding studies with Cu^{2+}, it would be interesting to study the effect of Cu^{2+} on the activity of the protein. Other metals shown to bind PAI-1 by IMAC, including Ni^{2+}, Zn^{2+} and Co^{2+}, could be tested as well.

An alternative method of assessing a change in PAI-1 activity and stability is the tPA assay, described in Chapter 3 for testing D-14-1B PAI-1 activity. This assay is essentially the same as the assay with trypsin, but the serine protease (tPA) is a cognate PAI-1 target.

It is possible that metals, especially one that binds well, like Cu^{2+}, might have an effect on PAI-1 activity toward tPA, even if there is no measurable effect toward trypsin.

CHAPTER 3

EXPRESSION, PURIFICATION AND TESTING OF PERDEUTERATED PAI-1

Introduction

As mentioned in Chapter 1, high-resolution structural information for vitronectin is lacking, in part due to some attributes that make vitronectin unsuited for the more common techniques of three-dimensional structural determination, i.e., NMR and x-ray crystallography. At 62-kDa, it is not a likely candidate for NMR studies; although two solution structures for the 5-kDa SMB domain of vitronectin have been solved by NMR [6, 7], this represents only a small portion of the entire protein. Glycosylations of vitronectin, along with its tendency to self-multimerize, hinder crystallization of the protein. A crystal structure has been solved for only the SMB domain, in complex with PAI-1 [8].

Other approaches have been used to provide additional structural information for vitronectin. Computational models from threading have been published for three main domains of vitronectin: the SMB domain; nearly 200 residues of the central domain; and the C-terminal domain, including the heparin binding region [10]. But these are only predictions and again cover only discrete regions of vitronectin, separate from the complete polypeptide. Three-dimensional structural information for the entirety of vitronectin is limited to a low-resolution model of the protein from SAXS [9]. Clearly,

alternative techniques must be employed to elucidate further structural details of vitronectin.

One alternative technique that our laboratory plans to apply to vitronectin and the Vn-PAI-1 complex is small-angle neutron scattering (SANS). Although such a technique is outside the scope of the work for this thesis, this work has provided one of the deuterated reagents, D-PAI-1, necessary to carry out these experiments.

The method of SANS, which relies on the ability of certain atomic nuclei to scatter incident neutrons, can provide the basic shape and size of a molecule in solution, with a resolution range of 10 – 1000 Å. Hydrogen and deuterium nuclei scatter neutrons differently, resulting in different scattering length densities. This difference directly affects the intensity of the detected, scattered neutron beam. In the two-phase system of a particle in a solvent, the difference in the scattering length densities of particle and solvent is referred to as "contrast." The scattering length density of the solvent can be varied by including D_2O, and changing the D_2O/H_2O ratio. Thus, the contrast can be adjusted to provide a more intense scattered neutron beam from the particle relative to that from the solvent, and the data collected can be used to produce a three-dimensional model of the particle.

Whereas SAXS also can provide size and shape information of about the same resolution, an advantage of SANS can be realized in analysis of a complex of different molecules, such as higher-order Vn-PAI-1 complexes. Using SANS, if one molecule is perdeuterated and the other is protonated, in addition to adjusting the solvent D_2O/H_2O ratio so that the entire complex can be differentiated from the solvent, the D_2O/H_2O ratio can be adjusted to allow only the protonated or only the deuterated species to be

differentiated from the solvent. This can provide information about the relative positions of each type of molecule in the complex. For Vn-PAI-1, SAXS can be used to determine the outer envelope of the complex, as well as the radius of gyration, and this information can aid in analysis of the SANS data. Because hydrogen and deuterium scatter x-rays the same, both proteins can be protonated for a SAXS experiment. Although vitronectin and PAI-1 in the complex analyzed by SAXS will be indistinguishable from each other, combining information from SAXS and SANS can reveal the locations of each protein relative to the other. Furthermore, comparing the shape of monomeric vitronectin obtained by SANS with the shape of vitronectin in complex with PAI-1 can provide information about conformational changes in vitronectin upon binding PAI-1. Similar changes are thought to occur in several other situations for vitronectin, including ECM deposition [68] and complex formation with thrombin-antithrombin [52]. Such conformational information may be widely applicable.

Since vitronectin is typically isolated from human plasma, and therefore cannot be deuterated, the recombinant PAI-1 must be deuterated for SANS experiments involving the complex. A recombinant bacterial expression system for PAI-1 was adapted to produce perdeuterated 14-1B PAI-1 (D-14-1B PAI-1), using a deuterated rich growth medium. D-14-1B PAI-1 was purified, characterized and assayed for activity. In addition, conditions were determined under which vitronectin, PAI-1, and the Vn-PAI-1 complex, are monodisperse and free from aggregation in solution, two aspects which are crucial to meaningful scattering measurements. The methods developed have already been used by others in our laboratory to prepare D-PAI-1 used in an initial set of SANS experiments.

D-PAI-1 can be used in other future work requiring deuterated protein – not only with additional SANS experiments, but also with NMR.

Materials and Methods

Materials

Plasmid DNA coding for wtPAI-1 (contained in the pET24d vector) and 14-1B PAI-1 (contained in the pEX vector) was a gift from Grant Blouse (Henry Ford Health System). Competent *Escherichia coli (E. coli)* cells, strain BL21(DE3) pLysS, were purchased from Novagen. Minimal medium with M9 salts was prepared according to Maniatis [69], with the additional components, $MgSO_4$, $CaCl_2$, biotin, and GIBCO MEM Vitamin solution (GIBCO). Celtone complete media, both unlabeled and deuterated, were from Spectra Stable Isotopes; Silantes rich media, both unlabeled and OD2[1] D (deuterated), were from Silantes GmbH. tPA and monoclonal antibody to PAI-1 were from Molecular Innovations; polyclonal anti-PAI-1 serum was a gift from Dr. Tom Podor. Peroxidase-linked anti-mouse antibody and anti-rabbit antibody were from Vector Labs.

Expression and Purification of Recombinant PAI-1 (wild-type and 14-1B mutant)

Plasmid DNA coding for wtPAI-1 or 14-1B PAI-1 was transformed into competent *E.coli* cells, strain BL21(DE3) pLysS, which were plated on agar with appropriate antibiotics: 30 μg/ml chloramphenicol and either 40 μg/ml kanamycin (pET24d) or 50 μg/ml ampicillin (pEX). After overnight growth at 37°C, transformants were grown in Luria broth (LB) at 30 or 37°C to mid-log phase, when PAI-1 expression was induced

[1] "OD2 D" is the name of rich media produced by Silantes. "OD2" indicates the level of cell density typically achieved, as measured by optical density.

with addition of isopropylthiogalactoside (IPTG) to 1.0 mM. After 3 to 6 hours, cells were harvested by centrifugation, resuspended in lysis buffer (50 mM Tris, pH 6.6, containing 100 mM NaCl and 1 mM EDTA), and lysed with three freeze-thaw cycles. The lysed cell suspension was centrifuged to pellet the cellular debris and insoluble proteins. The supernatant was diluted by 1/3 with Buffer A (50-mM potassium phosphate buffer, pH 6.6, containing 1 mM EDTA), followed by addition of 65% ammonium sulfate to precipitate the proteins. This suspension was centrifuged to pellet the proteins, and the pellet was resuspended in Buffer SB (50-mM potassium phosphate buffer, pH 6.6, containing 80 mM ammonium sulfate and 1 mM EDTA), and dialyzed against this buffer. The PAI-1 protein was isolated from this solution by successive column chromatography steps using heparin sepharose, phenyl sepharose, and sulfopropyl (SP) sepharose (Amersham Biosciences). The heparin sepharose column was equilibrated and washed (after sample loading) in Buffer SB; bound protein was eluted with a linear gradient to Buffer B (50-mM potassium phosphate buffer, pH 6.6, containing 1.15 M ammonium sulfate and 1 mM EDTA). PAI-1-containing fractions were pooled, the ammounium sulfate concentration was adjusted to approximately 1.15 M, and the sample was loaded on the phenyl sepharose column, which was equilibrated and washed in Buffer B, and eluted in a linear, reverse salt gradient to Buffer A. PAI-1-rich fractions were pooled and precipitated in 65% ammonium sulfate, resuspended in Buffer A, and loaded on the SP sepharose column, which had been charged with Buffer B, then equilibrated in Buffer SB. Following a wash in Buffer SB, PAI-1 was eluted in a linear gradient to Buffer C (50-mM potassium phosphate buffer, pH 6.6, containing 0.5 M ammonium sulfate and 1 mM EDTA). Protein purity was assessed by SDS-PAGE and

Western blot. PAI-1-rich fractions were pooled and dialyzed into storage buffer (5 mM sodium phosphate, pH 6.25, 0.35 M NaCl, 1 mM EDTA). Purified PAI-1 was stored at -80°C.

Expression of Deuterated 14-1B PAI-1

Transformation and competent cell growth were as described above for protonated 14-1B PAI-1. After overnight growth at 37°C, transformants were grown in Silantes OD2 D deuterated rich media at 30 or 37°C to mid-log phase, when 14-1B PAI-1 expression was induced with addition of IPTG to 1.0 mM. Expression was allowed to continue for 6 h. Cell harvest and lysing, as well as protein purification, were as described above for protonated PAI-1.

SDS-PAGE and Western Blotting

Proteins were electrophoresed on a 10% polyacrylamide SDS gel. Protein bands were visualized either by staining with Coomassie blue followed by destaining with glacial acetic acid and methanol, or by staining with GelCode Blue Stain Reagent (Pierce) followed by destaining with water. For Western blotting, after proteins were electrophoresed as above, they were transferred to a nitrocellulose membrane using a Semi-dry Transfer Cell (BioRad) in buffer consisting of 0.35 M glycine, 25 mM Tris, and 20% (v:v) methanol. The membrane was blocked against nonspecific antibody binding by incubation in 10% (w:v) nonfat dry milk in PBS. The membrane was washed three times in PBS containing 0.05% (v:v) Tween-20. The membrane was probed for PAI-1 by incubation in 2% nonfat dry milk in PBS containing an appropriately diluted murine monoclonal antibody to PAI-1 (1:25,000) or polyclonal anti-PAI-1 rabbit serum

(1:10,000), then washed three times as before. A horseradish peroxidase-linked anti-mouse antibody or anti-rabbit antibody, as appropriate, was applied as a 1:2,500 dilution in 2% nonfat dry milk in PBS. The membrane was washed as before, then the proteins were visualized by development in PBS containing 3 mg/ml 4-chloronaphthol in methanol and 0.05% (v:v) 30% H_2O_2.

tPA Activity Assay

Purified PAI-1 activity was assessed by its ability to inhibit tPA activity. An aliquot (10-20 μl) of PAI-1 was mixed with tPA having a final concentration of 0.2 μM in 25mM HEPES, pH 7.4, 0.135M NaCl, 1 mM EDTA. After a 10-min. incubation at 37°C, residual tPA activity was tested with addition of 100 μl of the PAI-1-tPA mixture to 900 μl Spectrozyme-tPA chromogenic substrate (American Diagnostica) having a final concentration of 90 μM. After 5 min. at 37°C, the reaction was quenched with acetic acid. The amount of cleaved substrate was determined by reading the sample absorbance at 405 nm.

PAI-1-tPA Binding Assay

To test PAI-1 for the ability to form a SDS-stable complex with tPA, the two proteins were mixed in a 1:2 PAI-1:tPA ratio and incubated at room temperature for 15 min. The binding reaction was quenched with addition of 0.1M HCl. Non-reducing gel-loading buffer was added, without boiling, followed by addition of 1M NaOH to return pH to basic. Fifty-microliter samples were loaded on a 10% SDS-polyacrylamide gel and electrophoresed, followed by staining with Coomassie blue.

Dynamic Light Scattering

Dynamic light scattering experiments were performed at Oak Ridge National Laboratory with a Wyatt Technology instrument, using a source wavelength of 690 nm. Vitronectin and PAI-1 were tested individually and as a complex, in phosphate-buffered saline (PBS) at pH 7.4, with either a physiological concentration of NaCl (0.15 M) or a high-salt concentration (0.31 M). To determine if high-molecular weight aggregates were present in the proteins, PAI-1 (molecular weight 43 kDa) was either filtered through a 100-kDa filter or unfiltered, and vitronectin (molecular weight 62 kDa) was filtered through either a 100-kDa filter, a 300-kDa filter, or no filter. For the complex, PAI-1 and vitronectin were added in equimolar concentrations, to give a total protein concentration of 0.7 mg/ml.

Results and Discussion

PAI-1 Expression and Purification

Active, deuterated 14-1B PAI-1 was successfully expressed in Silantes deuterated rich medium. The strategy for identifying a suitable growth medium was to compare growth and expression in three types of unlabeled media, followed by assessing growth and expression in deuterium-labeled media. The three types of unlabeled media were: minimal medium with M9 salts, Celtone complete medium, and Silantes rich medium. Compared to cell growth in LB, growth in unlabeled Celtone and Silantes was acceptable, while growth in minimal medium was very low. Figure 25 shows a comparison of cell density over time for LB, M9 minimal and Silantes, all unlabeled

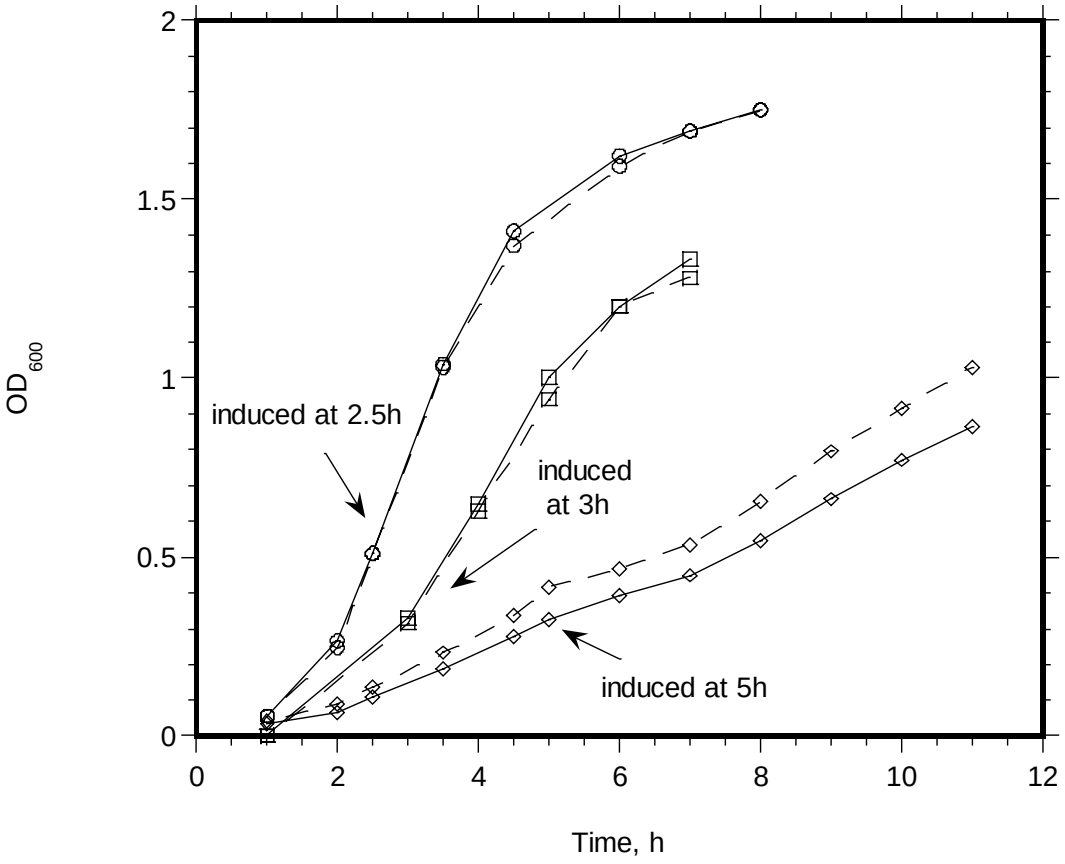


Figure 25: Growth curves for *E. coli* in unlabeled media.
Unlabeled versions of two potential deuteration media were compared for support of *E. coli* growth and PAI-1 expression. Growth and expression, both at 37°C, were in either LB (*circles*), Silantes unlabelled rich medium (*squares*), or M9 minimal medium, supplemented as described in *Materials and Methods* (*diamonds*). Because growth in Silantes unlabeled medium was superior to growth in unlabeled M9 medium, Silantes medium was chosen for expression of labeled (deuterated) PAI-1. Each data point represents a single sample. *Lines* are shown for clarity and do not represent fits to the data.

media. SDS gels and Western blots of cell lysates, after induction of PAI-1 expression, were used to assess PAI-1 expression. Expression levels in unlabeled M9 medium were deemed too low to expect useful protein expression in deuterated M9 medium; therefore this option was eliminated from consideration.

The protocol for Celtone growth requires adaptation of bacteria to gradually increasing levels of deuterium over five days, while fully deuterated Silantes medium can be inoculated directly with a small start-up culture after several hours of growth. Cells in Celtone failed to express PAI-1 protein. However, expression in Silantes was comparable to that in LB. Therefore, Silantes deuterated rich medium was chosen for growth and expression of D-PAI-1. The PAI-1 purification procedure was tested with 2-liter batches of LB-expressed protein, before 2-liter production of labeled Silantes-produced protein. Mass spectrometry analysis of D-PAI-1 produced in Silantes showed the protein to be approximately 86% deuterated, well above the minimum level of 70% deuterium incorporation required for SANS experiments.

PAI-1 Activity Testing

To test D-14-1B PAI-1 for activity, two assays were performed: one to test binding to its cognate serine protease, tPA; and one to test inhibitory activity toward tPA. In the tPA binding assay, PAI-1 is incubated with excess tPA, and the sample is electrophoresed on a polyacrylamide gel. Active PAI-1 forms an SDS-stable complex with tPA (the acyl-enzyme intermediate complex, which PAI-1 RCL insertion prevents from resolution by the protease), detectable by its migration position on the gel. D-14-1B-PAI-1 was shown to bind tPA, with very little unbound inhibitor remaining, indicating most of the isolated D-14-1B PAI-1 was active (Figure 26).

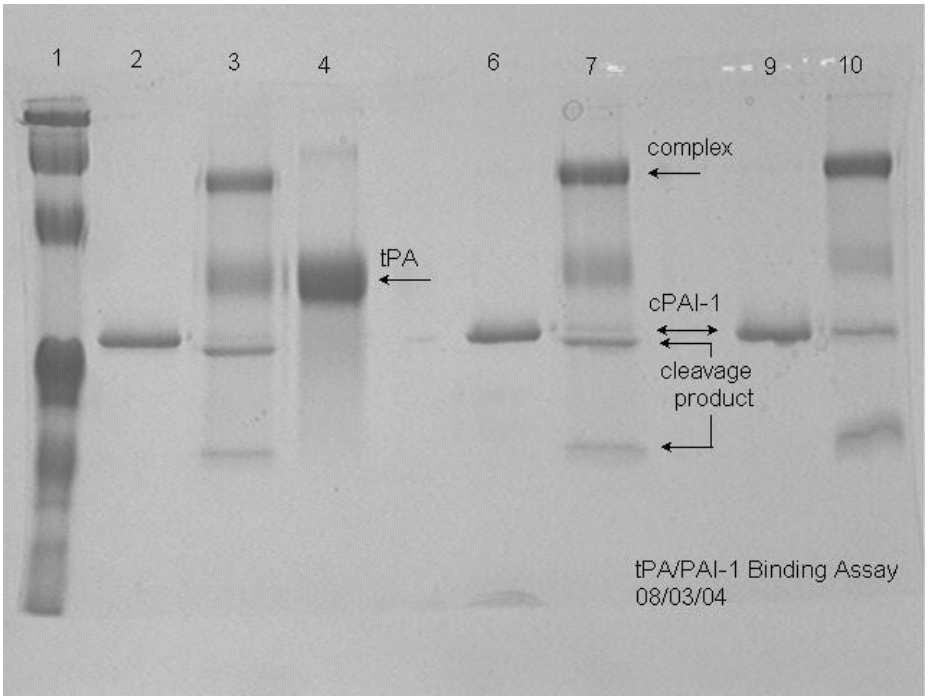


Figure 26: D-14-1B PAI-1 binding of tPA is comparable to H-14-1B PAI-1 binding of tPA.

PAI-1 was tested for the ability to form an SDS-stable complex with tPA, by mixing in a 1:2 PAI-1:tPA ratio and incubating at room temperature for 15 min. The binding reaction was quenched with addition of 0.1M HCl, and non-reducing gel-loading buffer was added, without boiling, followed by addition of 1M NaOH to return pH to basic. Fifty-microliter samples were analyzed by 10% SDS-polyacrylamide gel and electrophoresed, followed by staining with Coomassie blue. Presence of SDS-stable PAI-1-tPA complex indicates active PAI-1. *Lane 1*: Molecular weight standards; *lane 2*: D-14-1B PAI-1, sample #1; *lane 3*: tPA + D-14-1B PAI-1, sample #1; *lane 4*: tPA control; *lane 6*: D-14-1B PAI-1, sample #2; *lane 7*: tPA + D-14-1B PAI-1, sample #2; *lane 9*: commercial 14-1B PAI-1 control; *lane 10*: tPA + commercial 14-1B PAI-1 control.

The tPA inhibition assay uses a chromogenic tPA substrate. When the substrate is cleaved by tPA, its absorbance peak shifts; this can be measured spectrophotometrically. Active PAI-1 binds to tPA and inhibits cleavage of substrate, resulting in less color development. Both protonated and deuterated 14-1B PAI-1 were confirmed to be active by this assay, with absorbance by the cleaved substrate giving a clear concentration-dependent response to increasing PAI-1 concentration (Figure 27).

Confirmation of protein monodispersity

Crucial for meaningful neutron scattering experiments are monodisperse samples free from aggregates. Experimental conditions giving monodisperse, non-aggregated PAI-1, as well as vitronectin and Vn-PAI-1 complexes, were determined. To characterize the behavior of the proteins under various buffer and preparation conditions, dynamic light scattering (DLS) was used. Also known as quasi-elastic scattering, DLS measures time-dependent fluctuations in the scattered light. It gives a weighted average of the hydrodynamic radius (Rh) of macromolecules or particles in solution. A single Rh value that is reasonable for the macromolecular species of interest indicates the molecules to be monodisperse and not aggregated. For a 1:1 molar ratio of PAI-1 to vitronectin, at a total protein concentration of 0.7 mg/ml, acceptable conditions for monodispersity and lack of aggregation were found with buffer having 150 mM NaCl; PAI-1 filtered through a 100-kDa filter; and vitronectin filtered through a 300-kDa filter. These conditions have since been used by others in our laboratory for SANS experiments, and should be suitable for future SANS experiments. As an example of the data obtained by DLS, see Figure 28.

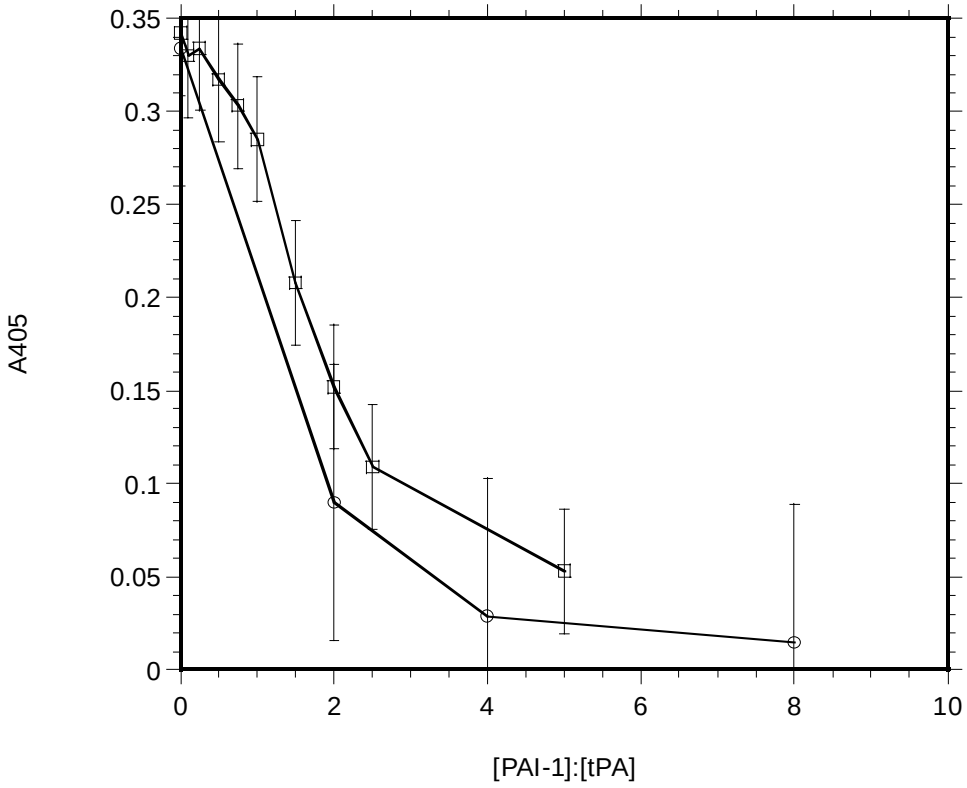


Figure 27: Activity of D-14-1B PAI-1 is comparable to activity of H-PAI-1.
Purified PAI-1 was assessed by its ability to inhibit tPA activity. Aliquots of increasing concentration of H-14-1B PAI-1 (*squares) or* D-14-1B PAI-1 (*circles)* were mixed with tPA having a final concentration of 0.2 μM in 25mM HEPES, pH 7.4, 0.135M NaCl, 1 mM EDTA. After a 10-min incubation at 37°C, residual tPA activity was measured using Spectrozyme-tPA chromogenic substrate, as described in *Materials and Methods*. The amount of cleaved substrate was determined by reading the sample absorbance at 405 nm. The decreasing trend in A_{405} vs. the increasing PAI-1:tPA molar ratio indicates active PAI-1. Each data point represents the average of two samples (H-14-1B PAI-1) or a single sample (D-14-1B PAI-1). *Lines* are shown for clarity and do not represent fits to the data. *Error bars* represent standard error.

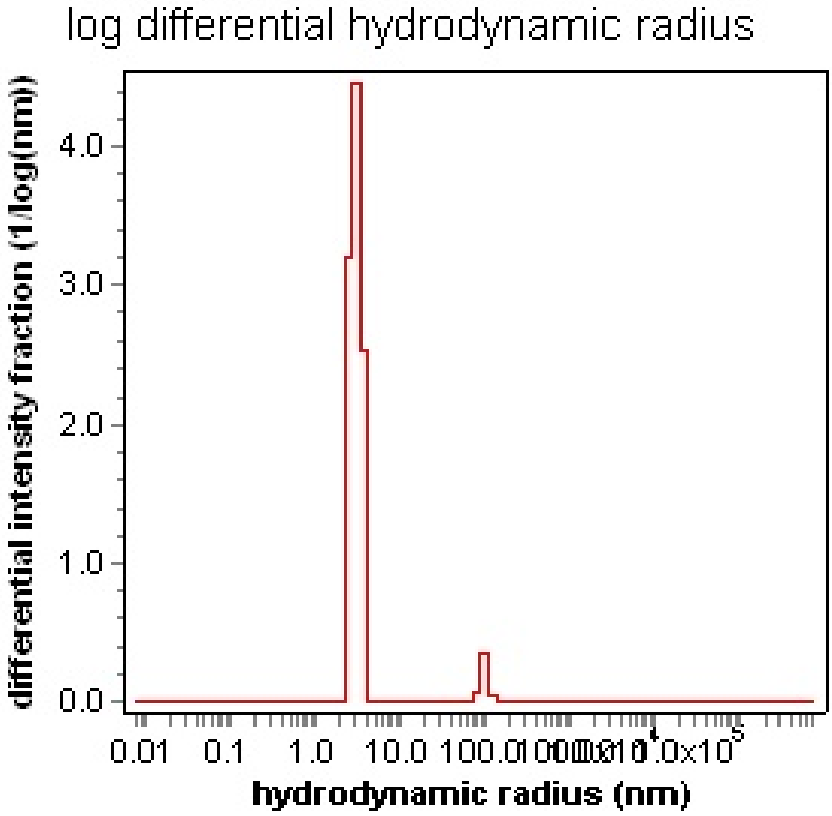


Figure 28: Dynamic light scattering characterization of PAI-1.
To test for aggregated PAI-1, using conditions planned for PAI-1 preparation for SANS experiments, dynamic light scattering was performed with a Wyatt Technology instrument using a source wavelength of 690 nm. PAI-1 was prepared in PBS, pH 7.4, 0.15 M NaCl, and filtered through a 100-kDa filter. The single, large peak indicates a monodisperse sample, free from aggregation, while the position of the peak at 3 nm indicates a reasonable Rh for PAI-1, a 43-kDa protein.

The single peak centered at Rh 3 nm for a sample of PAI-1, indicates monodispersity and a reasonable size for PAI-1.

Future Directions

The successful expression and purification of active, deuterated PAI-1 is an exciting step toward experiments that can yield structural information regarding the enigmatic Vn-PAI-1 complex. The methods developed for expression and purification of perdeuterated PAI-1 have already been used by others in our laboratory to prepare D-PAI-1 used in an initial set of SANS experiments, and can be used in other future work requiring deuterated PAI-1. Such future work is anticipated to include not only SANS but other experimental techniques as well. An example is NMR experimentation on the complex between vitronectin and PAI-1, to study the interface between deuterated PAI-1 and protonated vitronectin.

CHAPTER 4

CHARACTERIZATION OF MONOCLONAL ANTIBODIES TO VITRONECTIN AND CRYSTALLIZATION SCREEN OF VN-MAB COMPLEX

Introduction

As discussed in Chapter 1, alternative means of gaining structural insight into vitronectin are needed. To that end, another aim involves an effort to crystallize vitronectin in complex with a monoclonal IgG antibody (mAb) or with the F_{ab} fragment of a mAb. For this project, a panel of mAbs were screened for selection for use in crystallization trials, and an initial crystallization screen of Vn-mAb complex was set up.

Crystallization of the complex was chosen because an antibody molecule may help a bound protein form a lattice. A separate set of screens is planned for the complex with the F_{ab} fragment to take advantage of a different binding stoichiometry, with just one vitronectin binding to each F_{ab} fragment rather than two, as in the case of the intact antibody. Three examples of the successful use of F_{ab} fragments are the recent co-crystallization of a complex of the SMB domain of vitronectin, uPA, and uPAR (with anti-uPAR F_{ab} fragments) [70], and of two separate human immunodeficiency virus proteins [71-73].

A monoclonal rather than a polyclonal antibody was used because all molecules of a monoclonal antibody are the same, binding to the same epitope, while polyclonal antibodies contain a mixture of molecules which bind to different epitopes. Because

crystallization of molecules requires homogeneity of sample, all antibodies must bind the antigen, vitronectin, the same way.

The panel of mAbs screened offer the potential for many uses in our lab. The strategy for initial screening was interaction with both solid-phase (multimeric) and solution-phase (monomeric, native) vitronectin, via enzyme-linked immunosorbent assay (ELISA). Based on results of these assays, three antibodies were selected for Vn-mAb complex characterization by size-exclusion HPLC. Others in our lab also have tested some of the mAbs for reactivity with vitronectin in immunoblots.

Materials and Methods

Materials

Anti-vitronectin monoclonal antibodies were from either Molecular Innovations (1D1, 1E9, 2A10, 2C3, 4A1, 8H1), Green Mountain Antibodies, or Quidel. Peroxidase-linked anti-mouse IgG from horse was from Vector Labs. Recombinant PAI-1 was from Molecular Innovations. Native vitronectin was isolated from human plasma, as described in Chapter 2 of this work.

Non-competitive ELISA Titrations of Anti-vitronectin Monoclonal Antibodies

Polystyrene 96-well plates (CoStar) were coated with vitronectin (0.5 µg/ml, 100 µl/well) in 50 mM Na_2CO_3 buffer, pH 8.5, at room temperature for four hours or overnight. Plates were washed three times with TBS (20 mM Tris, 137 mM NaCl, 2.7 mM KCl, pH 7.4) then blocked with 2% (w:v) BSA (Fraction V; Sigma) in TBS at room temperature for one hour. Plates were washed as before. An anti-vitronectin monoclonal

antibody, diluted 1:250 in 0.2% BSA in TBS, was serially diluted 1:4 from row to row, with a final volume of 80 µl/well. (For antibodies that were found to result in a weak signal after plate development, the assay was repeated using 1:1 serial dilutions. For antibodies that resulted in a saturated signal at the original dilutions, the assay was repeated using starting antibody dilutions of 1:1000 or 1:6250.) Plates were incubated at room temperature for one hour before being washed as before. One-hundred microliters of secondary antibody (peroxidase-linked anti-mouse IgG from horse), diluted 1:1000 in 0.2% BSA in TBS, was added to each well and incubated at room temperature for one hour. Plates were washed as before, and then developed by addition of 100 µl developing solution [50 mM sodium citrate, pH5.5, 0.02% (w:v) ABTS, 0.05% (v:v) 30% H_2O_2] to each well. Absorbance at 405 nm was read on a Wallac Victor^2 1420 label counter, at five-minute intervals, up to 30 minutes.

Competitive ELISA Titrations of Anti-vitronectin Monoclonal Antibodies

Polystyrene 96-well plates (CoStar) were coated with vitronectin and blocked as for the non-competitive ELISA described above. A control for no antigen and no antibody was set up in one row with addition of 100 µl 0.2% BSA (in TBS) only. A control for no antigen was set up by filling another row with 50 µl 0.2% BSA plus 50 µl monoclonal antibody at the appropriate dilution (1:250, 1:1000 or 1:6250). A serial dilution of competing antigen – Vn – was set up by filling the next row with 100 µl of a 20 µg/ml solution of vitronectin in TBS containing 0.2% BSA, and filling subsequent rows with 50 µl 0.2% BSA in TBS. Fifty microliters from the antigen row was removed and serially diluted 1:1 in subsequent rows, with a final volume of 50 µl/well. Fifty microliters mAb

at the appropriate dilution was added to all rows containing vitronectin. Plates were incubated at room temperature for 1 hour, then washed three times as before. Addition of secondary antibody, development of plates, and absorbance reading were performed as described for the non-competitive assay above.

Characterization of Vn-mAb Complexes by HPLC

Size-exclusion HPLC, using a Phenomenex Biosep SEC-S3000 column (300 x 7.8 mm; MW range 5-700 kDa), attached to a Hewlett-Packard 1100 series HPLC system, was utilized to observe complex formation of vitronectin with monoclonal antibodies or with F_{ab}. Absorbance was detected in the instrument flow cell at 280 and 220 nm. The column was equilibrated with PBS, pH 7.4; flow rate was 0.5 ml/min. Vitronectin and mAb were mixed in molar ratios of 0.5:1, 1:1, 2:1, 2.5:1, 3:1 or 4:1; incubated at room temperature for 1 min; and 15 - 50 µl injected into the 50-µl loop. Fractions (0.5 ml or 0.25 ml) were analyzed by SDS-PAGE to confirm components of peaks.

Crystallization Screen of Vn-1E9 Complex

Both vitronectin and monoclonal antibody 1E9 were dialyzed into crystallization buffer (50 mM HEPES, pH 7.0, 0.15 M NaCl). Vitronectin at 3.6 mg/ml (58 µM) was mixed with 1E9 at 3.3 mg/ml (22 µM), giving a molar ratio of 2.6:1, Vn:1E9. One milliliter of the mixture (3.45 mg total protein) was loaded on an FPLC Superdex 200 column to isolate the complex by size exclusion; flow rate was 0.5 ml/min. Protein-rich fractions were identified by absorbance at 280 nm, and protein content of these fractions was analyzed by SDS-PAGE. Eight 1-ml fractions were pooled from the center of the elution peak shown to include both proteins. Containing a total of approximately 2 mg of

protein, the pool was concentrated to a final volume of 200 µl, for a concentration of 10 mg/ml. This sample and the screening components were equilibrated to room temperature to match the crystallization conditions, and crystallization screens were set up immediately.

The hanging drop vapor diffusion method was used to screen 120 different conditions in 24-well trays. For initial evaluation of protein solubility, the Classics Suite from Nextal Biotechnologies was used for 96 conditions. For another 24 conditions, to screen for preliminary crystallization conditions for intact antibodies, the Low Ionic Strength Screen from Hampton Research was used. The remaining 84 conditions included in the Hampton screen were postponed due to a lack of protein. Samples were monitored by light microscopy at set-up, and every few days for two weeks, then weekly for four weeks, then every few weeks, up to 10 months after setting up the screens.

SDS-PAGE

Proteins were electrophoresed on a 10% polyacrylamide SDS gel. Protein bands were visualized either by staining with Coomassie blue followed by destaining with glacial acetic acid and methanol, or by staining with GelCode Blue Stain Reagent (Pierce) followed by destaining with water.

Results and Discussion

Characterization of Antibodies by ELISA

Eight monoclonal antibodies specific for vitronectin were characterized with regard to their interaction with monomeric (native) and multimeric vitronectin, and the vitronectin-

PAI-1 complex. Non-competitive ELISA was used first to determine the working concentration of each antibody, *i.e.*, the concentration resulting in adequately strong binding to solid-phase vitronectin on the plate. These concentrations were used in competitive ELISAs to determine which antibodies bound well to native vitronectin in solution. Those that bound well showed a concentration-dependent decrease in binding to the solid-phase vitronectin, as the solution-phase vitronectin competed for mAb binding. Figures 29 and 30 show the ELISA results. Three mAbs – 1D1, 1E9, and a commercial antibody obtained from Green Mountain (GM) – clearly interact more strongly with both native and solid-phase vitronectin than do the others. This is reflected in the higher absorbance observed in the non-competitive ELISA, along with the decreasing absorbance seen as the native vitronectin concentration increases in the competitive ELISA.

Because of their superior interaction with vitronectin, antibodies 1D1, 1E9, and GM were selected for further evaluation of their suitability for co-crystallization screens. Four additional mAbs were selected for further assessment of their potential for other uses in our laboratory. These four mAbs were 2A10, 2C3, 8H1, and a commercial antibody obtained from Quidel (Q). Due to poor performance in both non-competitive and competitive ELISAs, mAb 4A1 was not tested further.

Characterization of Vn-mAb Complexes by HPLC

Size-exclusion HPLC was used for further analysis of Vn-mAb complex formation. Surprisingly, only one of the three candidates for co-crystallization screens formed complexes with vitronectin detectable by HPLC: 1E9. Samples of 1D1 or GM mAb incubated with vitronectin eluted as only two peaks, corresponding to free mAb and free

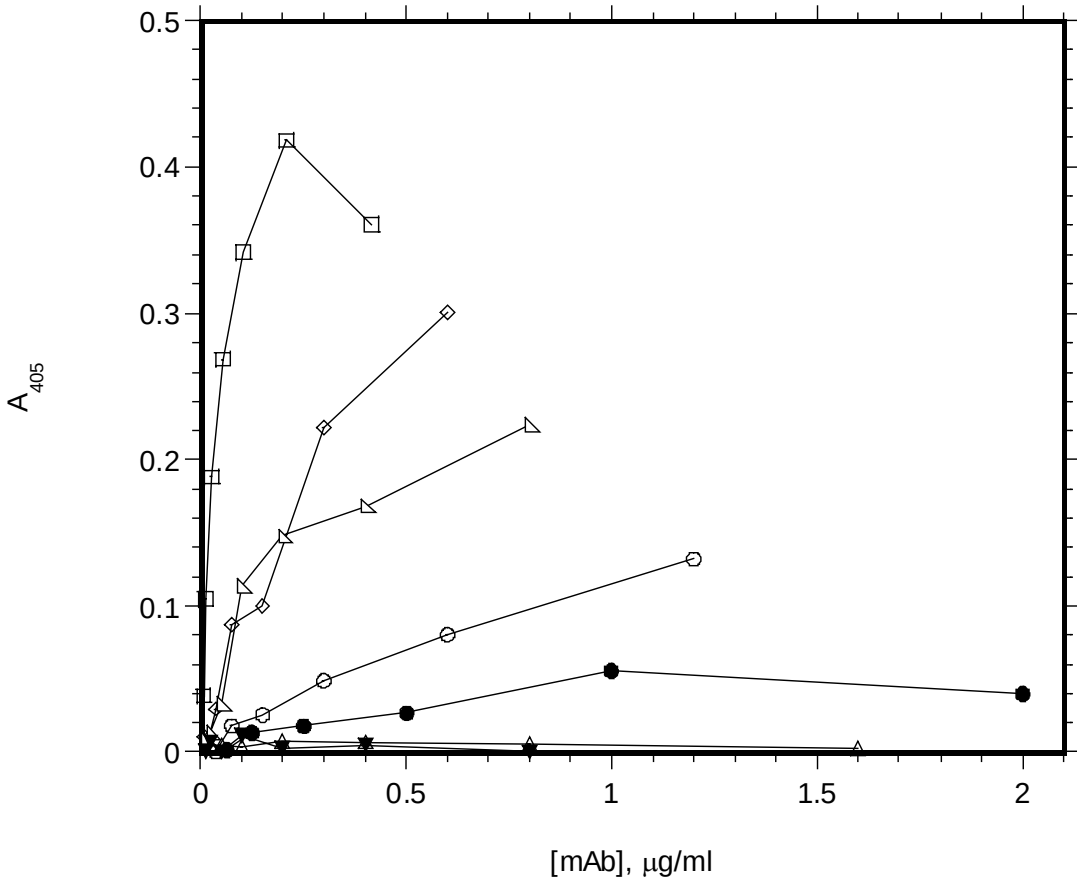


Figure 29: Anti-Vn mAb titrations by ELISA.
Monoclonal antibodies specific for Vn were tested for interaction with multimeric Vn (5 μg/ml) coated on ELISA plates. Each mAb was serially diluted and allowed to interact with Vn for 1 h; bound mAb was incubated with peroxidase-linked anti-mouse IgG for 1 h. Plates were developed with a solution containing ABTS and H_2O_2. Absorbance was read at 405 nm. MAbs tested include Q, *open circles;* GM, *open squares;* 1D1, *open diamonds;* 1E9, *open right triangles;* 2A10, *closed inverted triangles;* 4A1, *open triangles;* 8H1, *closed circles;* 2C3, *closed squares. Lines* are shown for clarity and do not represent fits to the data. For a given mAb concentration, a higher A_{405} indicates a more robust interaction of the mAb with multimeric Vn.

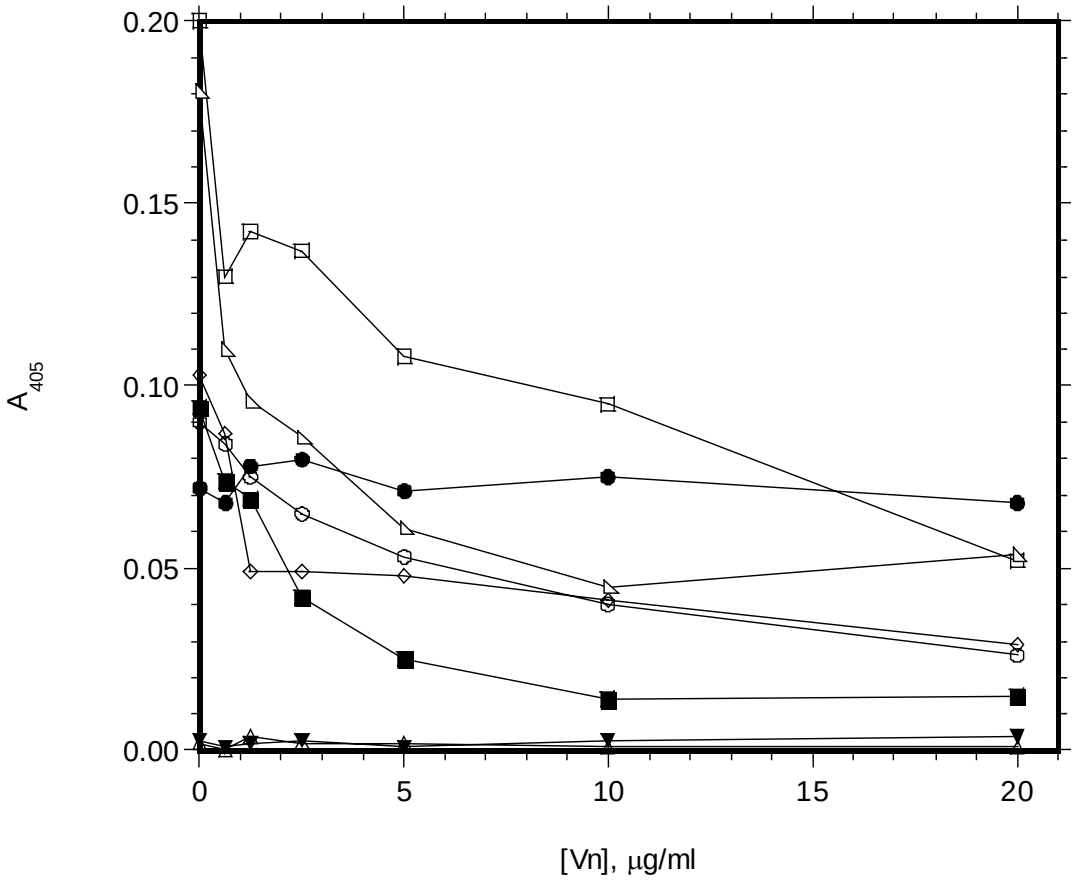


Figure 30: Anti-Vn mAb competitive ELISA.
Monoclonal antibodies specific for Vn were tested for interaction with native Vn. Each mAb was allowed to interact with serially diluted, native Vn (in solution) for 1 h in ELISA plates coated with multimeric Vn (5 μg/ml); mAb not captured by native Vn had the potential to bind to the Vn-coated plate. After the incubation with native Vn, bound mAb was incubated with peroxidase-linked anti-mouse IgG for 1 h. Plates were developed with a solution containing ABTS and H_2O_2. Absorbance was read at 405 nm. MAbs tested include Q, *open circles;* GM, *open squares;* 1D1, *open diamonds;* 1E9, *open right triangles;* 2A10, *closed inverted triangles;* 4A1, *open triangles;* 8H1, *closed circles;* 2C3, *closed squares. Lines* are shown for clarity and do not represent fits to the data. Decreasing A_{405} in response to increasing Vn in solution indicates interaction of mAb with native Vn. MAb concentrations used for competitive ELISAs, determined by titrations as described in the legend to Figure 28, were Q, 0.6 μg/ml; GM, 0.052 μg/ml; 1D1, 0.3 μg/ml; 1E9, 0.32 μg/ml; 2A10, 20 μg/ml; 4A1, 40 μg/ml; 8H1, 1.0 μg/ml; 2C3, 0.86 μg/ml.

vitronectin. In contrast, Vn-1E9 samples eluted as either two or three peaks, depending on the ratio of Vn:mAb; importantly, one peak always present corresponded to the complex. The chromatograms for the various Vn:mAb ratios tested, as well as for Vn and 1E9 alone, are shown in Figure 31.

The ratio of Vn:1E9 that produced the most complex and the least unbound proteins was 2:1. This was judged by a comparison of the peak heights relative to each other for each sample. The 2:1 sample had the highest peak corresponding to complex relative to the peaks corresponding to free proteins. Any increase in Vn greater than 2:1 resulted in an increase in only the peak from free Vn. For co-crystallization screens, all unbound protein must be removed to produce a homogeneous sample. This separation is most easily accomplished for samples containing minimal free protein. Therefore, 1E9 in a ratio of 2:1 Vn:mAb was selected for crystallization screens.

Besides 1E9, only 2C3 formed a complex with vitronectin that was detectable by HPLC analysis. However, the 2C3-Vn complex was present in only a small amount. Results of the characterization of the eight anti-vitronectin mAbs are summarized in Table 2.

Crystallization Screen of Vn-1E9 Complex

Purified Vn-1E9 complex was obtained by chromatographing a mixture of Vn and 1E9 on an FPLC Superdex 200 column. A successful peak separation can be seen on the chromatogram shown in Figure 32. The pool from the complex peak was concentrated to 10 mg/ml for the crystallization screen. The hanging drop vapor diffusion method was used to screen 120 different crystallization conditions for the purified complex of Vn-E9. Samples were monitored by light microscopy at set-up, and up to 10 months later.

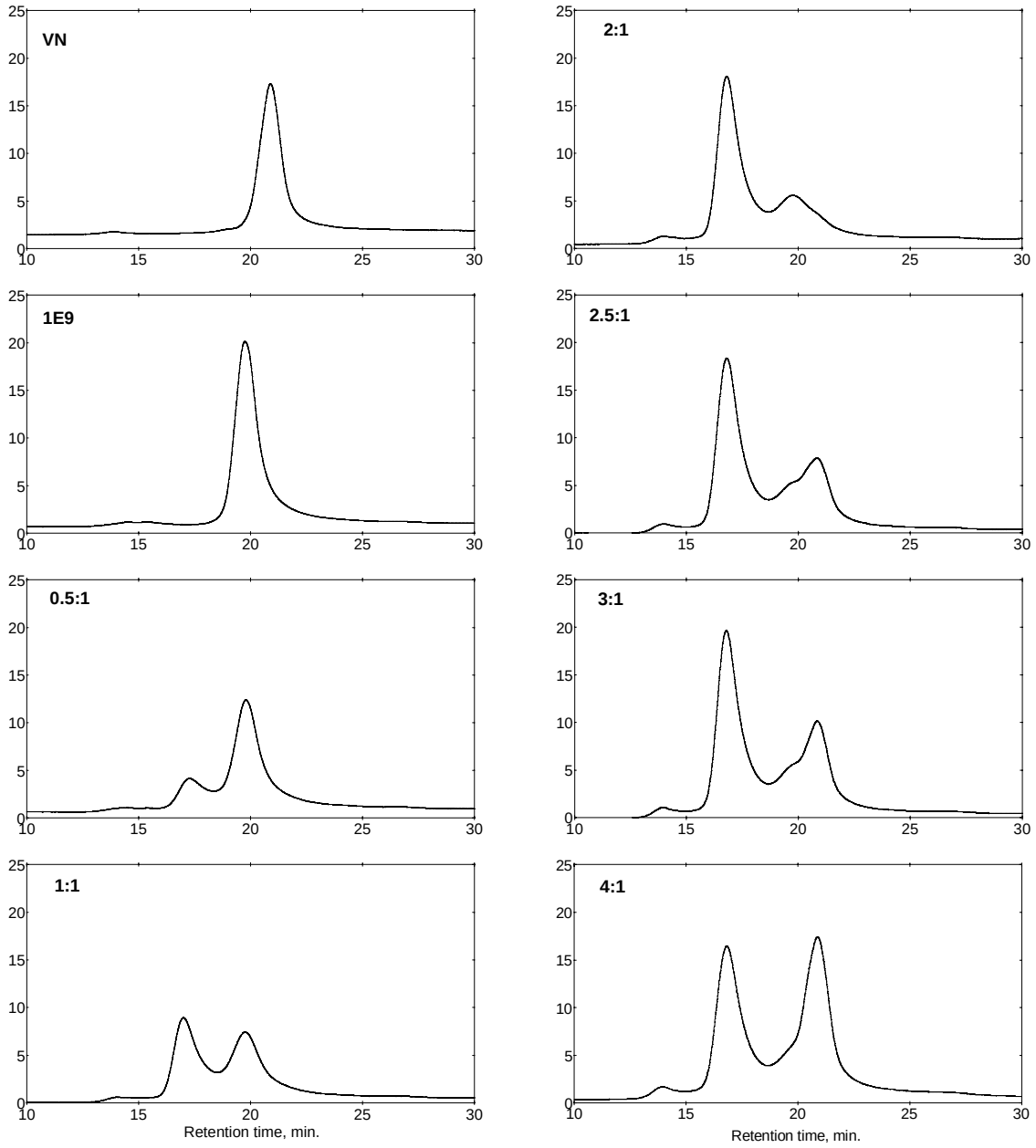


Figure 31: Size-exclusion HPLC analysis of Vn-1E9 complex formation.
Proteins were mixed in the molar ratios indicated (Vn:1E9) and incubated for one min before loading column (Phenomenex Biosep SEC-S3000 column, 300 x 7.8 mm) with 15 - 50 µl sample via a 50-µl loop. Column was equilibrated in PBS, pH 7.4; flow rate was 0.5 ml/min. Retention times, in min: Vn, 20.9; 1E9, 19.8; complex, 16.8-17.3. The 2:1 Vn:1E9 sample produced the most complex with the least unbound protein.

Table 2: Summary of anti-vitronectin mAb characterization

Vn mAb	Non-competitive ELISA	Competitive ELISA	HPLC Size-exclusion
1D1	Good Binding	Competition	No Complex
1E9	Good Binding	Competition	Complex
2A10	No Binding	Unsuitable (No plate binding)	*No Complex
2C3	Moderate Binding	Competition	*Complex (small amount)
4A1	No Binding	Unsuitable (No plate binding)	Not Tested
8H1	Weak Binding	No Competition	No Complex
Green Mtn	Good Binding	Competition	No Complex
Quidel	Moderate Binding	Competition	Inconclusive

*Data for HPLC analysis of 2A10 and 2C3 provided by Anand Mayasundari.

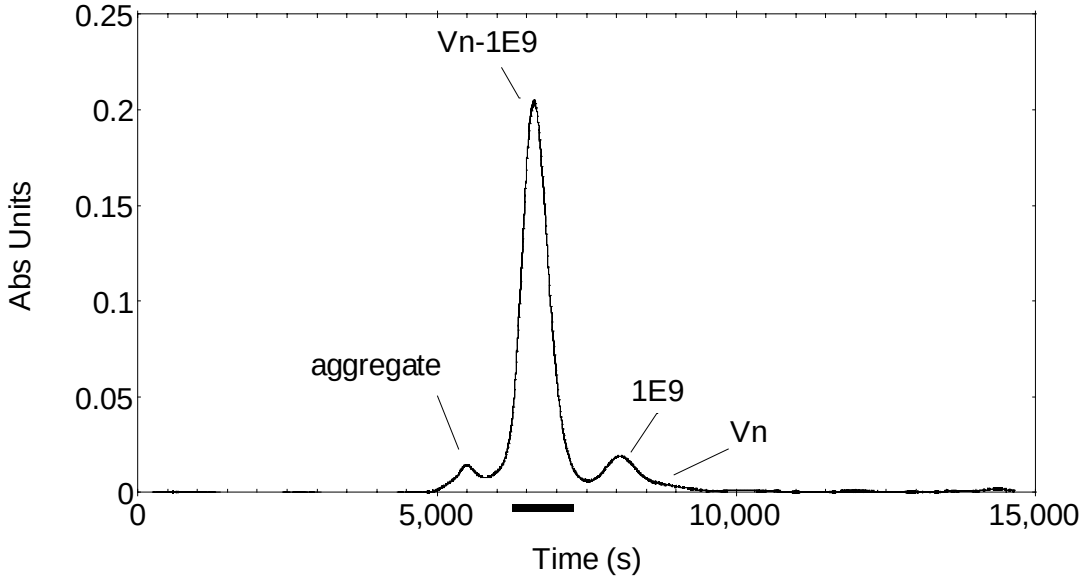


Figure 32: Size-exclusion FPLC isolation of Vn-1E9 complex for crystallization screen.

Vitronectin (58 μM) and mAb 1E9 (22 μM), both prepared in 50 mM HEPES, pH 7.0, 0.15 M NaCl, were mixed in a molar ratio of 2.6:1. The complex was isolated by size-exclusion chromatography of the mixture on an FPLC Superdex 200 column with a flow rate of 0.5 ml/min. Protein-rich fractions were identified by absorbance at 280 nm. Protein content of each chromatogram peak, confirmed by SDS-PAGE, is indicated. Fractions from the Vn-1E9 peak (indicated by the *bar*) were pooled, concentrated, and used to set up a crystallization screen, as described in *Materials and Methods*.

However, no conditions produced formations promising enough to warrant condition optimization. This is not surprising, given that intact IgGs have a hinge region that makes the molecule flexible. Complex formation with IgG fragments, such as F_{ab} or F_v, which do not have the hinge region, is more commonly used for attempted crystallizations [71].

Concluding Remarks and Future Directions

The characterization of a panel of eight monoclonal antibodies to vitronectin resulted in selection of mAb 1E9 for co-crystallization screens with vitronectin. Although the initial screens did not produce crystals, the same antibody can be used to provide F_{ab} fragments for a future co-crystallization screen with vitronectin. This option is promising because the F_{ab} fragment does not have the flexible hinge region of the intact antibody, and it offers a different stoichiometry due to its single binding site.

The information gained from the characterization of these antibodies will be valuable to our laboratory in the future. For example, strategic choices can be made about their use in immunoblotting, plate assays, and surface plasmon resonance binding experiments. Additional characterization of these antibodies that would be useful is epitope mapping of their binding sites on vitronectin.

List of References

1. Hayman, E.G., et al., *Serum Spreading Factor (vitronectin) is Present at the Cell Surface and in Tissues.* Proc Natl Acad Sci U S A, 1983. **80**: p. 4003-07.
2. Barnes, D. and J. Silnutzer, *Isolation of Human Serum Spreading Factor.* J Biol Chem, 1983. **258**: p. 12548-52.
3. Preissner, K.T., R. Wassmuth, and G. Muller-Berghaus, *Physicochemical characterization of human S-protein and its function in the blood coagulation system.* Biochem J, 1985. **231**: p. 349-55.
4. Preissner, K.T., *The role of vitronectin as multifunctional regulator in the hemostatic and immune systems.* Blut, 1989. **59**(5): p. 419-31.
5. Preissner, K.T., *Structure and biological role of vitronectin.* Annu Rev Cell Biol, 1991. **7**: p. 275-310.
6. Mayasundari, A., et al., *The Solution Structure of the N-terminal Domain of Human Vitronectin: PROXIMAL SITES THAT REGULATE FIBRINOLYSIS AND CELL MIGRATION.* J Biol Chem, 2004. **279**(28): p. 29359-29366.
7. Kamikubo, Y., et al., *Disulfide bonding arrangements in active forms of the somatomedin B domain of human vitronectin.* Biochemistry, 2004. **43**: p. 6519-34.
8. Zhou, A., et al., *How vitronectin binds PAI-1 to modulate fibrinolysis and cell migration.* Nat Struct Biol, 2003. **10**: p. 541-544.
9. Lynn, G.W., et al., *A Model for the Three-Dimensional Structure of Human Plasma Vitronectin from Small-Angle Scattering Measurements.* Biochemistry, 2005. **44**(2): p. 565-574.
10. Xu, D., et al., *Model for the three-dimensional structure of vitronectin: predictions for the multi-domain protein from threading and docking.* Proteins, 2001. **44**: p. 312-20.
11. Suzuki, et al., *Domain Structure of Vitronectin - Alignment of Active Sites.* J Biol Chem, 1984. **259**: p. 15307-14.
12. Horn, N.A., et al., *Assignment of the Four Disulfides in the N-terminal Somatomedin B Domain of Native Vitronectin Isolated from Human Plasma.* J Biol Chem, 2004. **279**(34): p. 35867-35878.
13. Kamikubo, Y., Y. Okumura, and D.J. Loskutoff, *Identification of the disulfide bonds in the recombinant somatomedin B domain of human vitronectin.* J Biol Chem, 2002. **277**: p. 27109-27119.
14. Royle, G., et al., *A method for defining binding sites involved in protein-protein interactions: analysis of the binding of plasminogen activator inhibitor 1 to the somatomedin domain of vitronectin.* Anal Biochem, 2001. **296**(2): p. 245-53.
15. Suzuki, et al., *Complete amino acid sequence of human vitronectin deduced from cDNA. Similarity of cell attachment sites in vitronectin and fibronectin.* EMBO J, 1985. **4**: p. 2519-24.
16. Zhao, Y. and D.C. Sane, *The cell attachment and spreading activity of vitronectin is dependent on the Arg-Gly-Asp sequence. Analysis by construction of RGD and domain deletion mutants.* Biochem Biophys Res Commun, 1993. **192**(2): p. 575-82.

17. Cherny, R.C., M.A. Honan, and P. Thiagarajan, *Site-directed mutagenesis of the arginine-glycine-aspartic acid in vitronectin abolishes cell adhesion.* J Biol Chem, 1993. **268**(13): p. 9725-9.
18. Stanley, K.K., *Homology with hemopexin suggests a possible scavenging function for S-protein/vitronectin.* FEBS Lett, 1986. **199**: p. 249-53.
19. Faber, H.R., et al., *1.8 A crystal structure of the C-terminal domain of rabbit serum haemopexin.* Structure, 1995. **3**(6): p. 551-9.
20. Hrkal, Z., et al., *Hyaluronan-binding properties of human serum hemopexin.* FEBS Lett, 1996. **383**: p. 72-4.
21. Preissner, K.T. and G. Muller-Berghaus, *S protein modulates the heparin-catalyzed inhibition of thrombin by antithrombin III. Evidence for a direct interaction of S protein with heparin.* Eur J Biochem, 1986. **156**(3): p. 645-50.
22. Schar, C.R., et al., *A Deletion Mutant of Vitronectin Lacking the Somatomedin B Domain Exhibits Residual Plasminogen Activator Inhibitor-1-binding Activity.* J Biol Chem, 2008. **283**(16): p. 10297-10309.
23. Erickson, L.A., M.H. Ginsberg, and D.J. Loskutoff, *Detection and Partial Characterization of an Inhibitor of Plasminogen Activator in Human Platelets.* J Clin Invest, 1984: p. 1465-71.
24. Chmielewska, J., et al., *On the relationship between different forms of the fast inhibitor of tissue plasminogen activator.* Fibrinolysis, 1987. **1**: p. 67-73.
25. Alessi, M.C., et al., *Purification and characterization of natural and recombinant human plasminogen activator inhibitor-1 (PAI-1).* Euro J Biochem, 1988. **175**: p. 531-40.
26. Declerck, P.J., et al., *Purification and characterization of a plasminogen activator inhibitor 1 binding protein from human plasma. Identification as a multimeric form of S protein (vitronectin).* J Biol Chem, 1988. **263**: p. 15454-61.
27. Stout, T.J., et al., *Structures of Active and Latent PAI-1: A Possible Stabilizing Role for Chloride Ions.* Biochemistry, 2000. **39**(29): p. 8460-8469.
28. Mottonen, J., et al., *Structural basis of latency in plasminogen activator inhibitor-1.* Nature, 1992. **355**(6357): p. 270-3.
29. Schar, C.R., et al., *Characterization of a Site on PAI-1 that Binds to Vitronectin Outside the Somatomedin B Domain.* submitted for publication, 2008.
30. Eagle, H., *Nutrition Needs of Mammalian Cells in Tissue Culture.* Science, 1955. **122**: p. 501-4.
31. Barnes, D. and G. Sato, *Growth of a human mammary tumour cell line in a serum-free medium.* Nature, 1979. **281**: p. 388-9.
32. Holmes, R., *Preparation from human serum of an alpha-one protein which induces the immediate growth of unadapted cells in vitro.* J Cell Bio, 1967. **32**: p. 297-308.
33. Westermark, B., Ã. Wasteson, and K. Uthne, *Initiation of DNA Synthesis of Stationary Human Glia-Like Cells by a Polypeptide Fraction from Human Plasma Containing Somatomedin Activity.* Experimental Cell Research, 1975. **96**: p. 58-62.

34. Fryklund, L. and H. Sievertsson, *Primary structure of somatomedin B: a growth hormone-dependent serum factor with protease inhibiting activity.* FEBS Lett, 1978. **87**: p. 55-60.
35. Heldin, C.-H., et al., *Somatomedin B: Mitogenic Activity Derived from Contaminant Epidermal Growth Factor.* Science, 1981. **213**(4512): p. 1122-1123.
36. Kolb and Muller-Eberhard, *The Membrane Attack Mechanism of Complement - Isolation and Subunit Composition of the C5b-9 Complex.* J Experimental Med, 1975. **141**: p. 724-35.
37. Podack, E., W. Kolb, and H. Muller-Eberhard, *The SC5b-7 Complex: Formation, Isolation, Properties, and Subunit Composition.* J Immunology, 1977. **119**: p. 2024-29.
38. Podack, E., Fed Proc, 1977.
39. Podack, E., W. Kolb, and H. Muller-Eberhard, *The C5b-6 Complex: Formation, Isolation, and Inhibition of Activity by Lipoprotein and the S-Protein of Human Serum.* J Immunology, 1978. **120**(1841-48).
40. Podack, E., et al., *The C5b-6 Complex: Reaction with C7, C8, C9.* J Immunology, 1978. **121**: p. 484-90.
41. Dahlback and Podack, *Characterization of Human S-Protein, an Inhibitor of the MAC of Complement. Demonstration of a Free Reactive Thiol Group.* Biochemistry, 1985. **24**: p. 2368-74.
42. Bittorf, S.V., E.C. Williams, and D.F. Mosher, *Alteration of vitronectin. Characterization of changes induced by treatment with urea.* J Biol Chem, 1993. **268**(33): p. 24838-46.
43. Podack, E. and H. Muller-Eberhard, *Isolation of Human S-Protein, an Inhibitor of the Membrane Attack Complex of Complement.* J Biol Chem, 1979. **254**: p. 9908-14.
44. Jenne, D., F. Hugo, and S. Bhakdi, *Interaction of complement S-protein with thrombin-antithrombin complexes: a role for the S-protein in haemostasis.* Thromb Res, 1985. **38**(4): p. 401-12.
45. Barnes, D., et al., *Effects of a serum spreading factor on growth and morphology of cells in serum-free medium.* J Supramol Struct, 1980. **14**: p. 47-63.
46. Knox, P. and S. Griffiths, *The distribution of cell-spreading activities in sera: a quantitative approach.* J Cell Sci, 1980. **46**: p. 97-112.
47. Knox and Whateley, 1980.
48. Knox, P., *Kinetics of cell spreading in the presence of different concentrations of serum or fibronectin-depleted serum.* J Cell Sci, 1984. **71**: p. 51-9.
49. Hayman, E.G., et al., *Cell Attachment on Replicas of SDS Polyacrylamide Gels Reveals Two Adhesive Plasma Proteins.* J Biol Chem, 1982. **95**: p. 20-23.
50. Barnes, D., et al., *Characterization of human serum spreading factor with monoclonal antibody.* Proc Natl Acad Sci U S A, 1983. **80**: p. 1362-66.
51. Barnes, D., J.E. Reing, and B. Amos, *Heparin-binding Properties of Human Serum Spreading Factor.* J Biol Chem, 1985. **260**: p. 9117-22.

52. Hogasen, *Heparin-binding properties of vitronectin are linked to complex formation as illustrated by in vitro polymerization and binding to the terminal complement complex.* J Biol Chem, 1992. **267**(32): p. 23076-82.
53. Hayashi, M., et al., *Activation of Vitronectin (Serum Spreading Factor) Binding of Heparin by Denaturing Agents.* J Biochem (Tokyo), 1985. **98**: p. 1135-8.
54. Ishikawa-Sakurai, M. and M. Hayashi, *Two collagen-binding domains of vitronectin.* Cell Struct Funct, 1993. **18**: p. 253-9.
55. Zhuang, P., M.N. Blackburn, and C.B. Peterson, *Characterization of the Denaturation and Renaturation of Human Plasma Vitronectin. I. BIOPHYSICAL CHARACTERIZATION OF PROTEIN UNFOLDING AND MULTIMERIZATION.* J Biol Chem, 1996. **271**: p. 14323-32.
56. Jenne, D. and K.K. Stanley, *Molecular cloning of S-protein, a link between complement, coagulation and cell-substrate adhesion.* Embo J, 1985. **4**: p. 3153-57.
57. Tomasini, B.R. and D.F. Mosher, *On the Identity of Vitronectin and S-Protein: Immunological Crossreactivity and Functional Studies.* Blood, 1986. **68**: p. 737-42.
58. Minor, K. and C.B. Peterson, *Plasminogen Activator-Inhibitor Type-1 Promotes the Self-Association of Vitronectin into Complexes Exhibiting Altered Incorporation into the Extracellular Matrix.* J Biol Chem. **277**: p. 10337-45.
59. Moreland, J.L., et al., *The Molecular Biology Toolkit (mbt): A Modular Platform for Developing Molecular Visualization Applications.* BMCBioinformatics, 2005. **6**: p. 21.
60. Rakhit, G. and B. Sarkar, *Electron spin resonance study of the copper(II) complexes of human and dog serum albumins and some peptide analogs.* J Inorg Biochem, 1981. **15**: p. 233-41.
61. Zhang, Y. and D. Wilcox, *Thermodynamic and spectroscopic study of Cu(II) and Ni(II) binding to bovine serum albumin.* J Biol Inorg Chem, 2002. **7**: p. 327-37.
62. Zgirski, A. and E. Frieden, *Binding of Cu(II) to Non-Prosthetic Sites in Ceruloplasmin and Bovine Serum Albumin.* J Inorg Biochem, 1990. **39**: p. 137-48.
63. Rozga, M., et al., *Human serum albumin coordinates Cu(II) at its N-terminal binding site with 1 pM affinity.* J Biol Inorg Chem, 2007. **12**: p. 913-18.
64. Bal, W., et al., *Multi-metal binding site of serum albumin.* J Inorg Biochem, 1998. **70**: p. 33-39.
65. Gibson, A.D. and C.B. Peterson, *Full-length and truncated forms of vitronectin provide insight into effects of proteolytic processing on function.* Biochim Biophys Acta, 2001. **1545**: p. 289-304.
66. Wojciech, B., et al., *Multi-metal binding site of serum albumin.* J Inorg Biochem, 1998. **70**: p. 33-39.
67. Mash, H., et al., *Complexation of Copper by Zwitterionic (Good) Buffers.* Anal Chem, 2003. **75**: p. 671-77.
68. Minor, K.H. and C.B. Peterson, *Plasminogen Activator Inhibitor Type 1 Promotes the Self-association of Vitronectin into Complexes Exhibiting Altered Incorporation into the Extracellular Matrix.* J Biol Chem, 2002. **277**(12): p. 10337-10345.

69. Sambrook, J., E. Fritsch, and T. Maniatis, *Molecular Cloning, A Laboratory Manual*, ed. C. Nolan. 1989: Cold Spring Harbor Laboratory Press.
70. Huai, Q., et al., *Crystal structures of two human vitronectin, urokinase and urokinase receptor complexes.* Nat Struct Mol Biol, 2008. **15**(422-423).
71. Kovari, L.C., C. Momany, and M.G. Rossmann, *The use of antibody fragments for crystallization and structure determinations.* Structure, 1995. **3**(12): p. 1291-1293.
72. Jacobo-Molina, A., et al., *Crystal Structure of Human Immunodeficiency Virus Type 1 Reverse Transcriptase Complexed with Double-Stranded DNA at 3.0 A Resolution Shows Bent DNA.* Proc Natl Acad Sci U S A, 1993. **90**(13): p. 6320-6324.
73. Prongay, A., et al., *Preparation and Crystallization of a Human Immunodeficiency Virus p24-Fab Complex.* Proc Natl Acad Sci U S A, 1990. **87**(24): p. 9980-9984.

Vita

Cynthia Lee Brown, known familiarly as Cindy, was born in Clarksville, TN. She attended The Clarksville Academy for grades 1-12, and graduated as class valedictorian. Having accepted a four-year scholarship to study engineering at the University of Tennessee, Knoxville, Cindy earned a BS degree there in Industrial Engineering. She worked as an engineer in the automotive parts manufacturing field for several years before returning to the University of Tennessee to study biology, with plans to earn a graduate degree and begin a career as a research scientist.